Accepted Manuscript

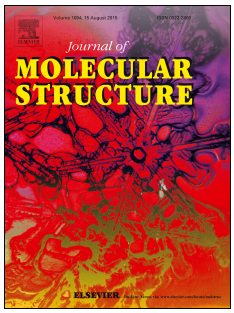

Synthesis, crystal structure, spectroscopic properties and potential anti-cancerous activities of four unsaturated bis-norcantharimides

Shuang-Shuang Cheng, Yan Shi, Xiao-Na Ma, Dian-Xiang Xing, Lian-Dong Liu, Yun Liu, Yun-Xue Zhao, Qi-Cheng Sui, Xue-Jie Tan

PII: S0022-2860(16)30187-9

DOI: 10.1016/j.molstruc.2016.02.093

Reference: MOLSTR 22302

To appear in: *Journal of Molecular Structure*

Received Date: 2 February 2016

Revised Date: 25 February 2016

Accepted Date: 25 February 2016

Please cite this article as: S.-S. Cheng, Y. Shi, X.-N. Ma, D.-X. Xing, L.-D. Liu, Y. Liu, Y.-X. Zhao, Q.-C. Sui, X.-J. Tan, Synthesis, crystal structure, spectroscopic properties and potential anti-cancerous activities of four unsaturated bis-norcantharimides, *Journal of Molecular Structure* (2016), doi: 10.1016/j.molstruc.2016.02.093.

Synthesis, crystal structure, spectroscopic properties and potential anti-cancerous activities of four unsaturated bis-norcantharimides

Shuang-Shuang Cheng [a], Yan Shi [a], Xiao-Na Ma [a], Dian-Xiang Xing [a], Lian-Dong Liu [b], Yun Liu [a], Yun-Xue Zhao [c], Qi-Cheng Sui [a], Xue-Jie Tan [a] *

[a] *School of Chemistry and Pharmaceutical Engineering, Qilu University of Technology, Jinan, Shandong Province, 250353, P. R. China*

[b] *College of Chemistry, Chemical Engineering and Materials Science, Shandong Normal University,* Jinan, *Shandong Province,* 250014, P. R. China

[c] *Department of Pharmacology, School of Medicine , Shandong University, Jinan,* Shandong Province, *250012, P. R. China*

ARTICLE INFO

Article history:
Received
Received in revised form
Accepted
Available online

Keywords:
Unsaturated norcantharimide dimers
Synthesis
Characterization
Single crystal structure
Cytotoxic activity

ABSTRACT

Four unsaturated norcantharimide (**UNCI**) dimers were synthesized and characterized by elemental analysis, ESI-QTOF-MS, FT/IR, UV–Vis, ^{1}H and ^{13}C NMR as well as single crystal X-ray diffraction. In addition, theoretical studies have been investigated to compare with the experimental findings. Introduction of various lengths of single bond link chains provides high conformational flexibility and thus unusual molecular and crystal structures for dimers. Two of the four dimers twist into helicate, but crystallize into centrosymmetric lattice; one adopts approximately centrosymmetric conformer, but packs into non-centrosymmetric polar space group ($P2_1$). Moreover, in vitro cytotoxic activities of four **UNCI** dimers and their corresponding saturated **NCI** dimers were evaluated. All four **UNCI** dimers are inactive and one **NCI** dimer shows modest cytotoxicity. These findings were compared with the relevant results in literatures. It is found that the antitumor properties of **UNCI/NCI** dimers depend mainly on the length of link chains (the longer chain, the higher therapeutic efficacy) and have relationship with the double bond, which requires more experimental support.

1. Introduction

As archetypal small molecule protein phosphatase inhibitors, [1] cantharidin (**CAN**) and norcantharidin (a demethylated form of cantharidin, also called demethylcantharidin, so abbreviated as **DMC**, **Scheme 1**) have been used worldwide as an anticancer agent since 1264 for the treatment of hepatoma, leukemia, pancreatic cancer, colon cancer, oral carcinoma, bladder cancer, breast cancer, lung cancer and digestive tract tumors [2]. Their ability to act against multidrug-resistant cells makes it an ideal compound for individualized cancer treatment [3]. Similarly, **CAN** possesses cytotoxicity to a series of normal cells, including gastrointestinal tract, urethra and kidney [2d], which delayed their use in the pharmaceutical industry. However, the organic chemistry has provided new and more potent derivatives with high activity against protein phosphatase enzyme and less toxicity profiles.

During the last five decades, thousands of analogues and derivatives have been synthesized and thoroughly investigated [2e], including **DMC**-platinum complexes [2b, 2c, 4], (nor)cantharimide series (abbreviated as **CAI/NCI**, **Scheme 1**) [2m, 5], anhydride ring-opened series (especially those with only one free carboxylate) [1g, 6] and so on. These analogues have demonstrated all kinds of antitumor activities and each has its own specific activity. Due to the possibility to incorporate any kinds of substituent in the nitrogen, as well as essentially equipotent inhibitory activity of the serine/threonine protein phosphatases 1 and 2A (PP1 and PP2A) with **CAN** (more potent than **DMC**) [7], **CAI/NCI** series show higher anticancer activities, and have been shown to inhibit xanthenes oxidase and to have antiplatelet effects on thrombin, arachidonic acid, collagen, and platelet-activating factor-induced aggregation [8]. So, derivatives of modified **CAI/NCI** are potentially useful as anticancer agents.

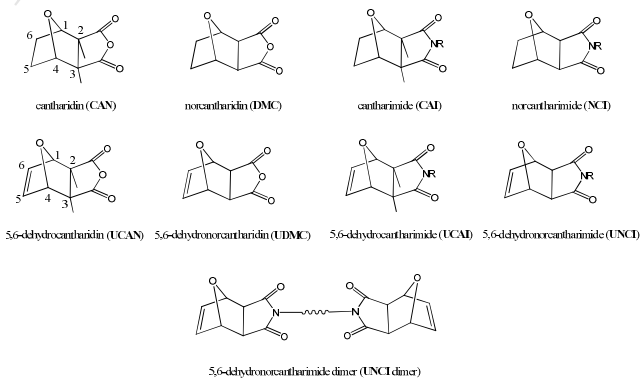

Scheme 1. Some important core structures of cantharidine analogues

As we know, the type of heteroatoms in the bridge and in the anhydride cycle are very important, but, the presence of double bond (5,6-ene) has little effect on activity [5d, 7, 9]. 5,6-dehydrocantharidin (the unsaturated analogue of **CAN,** abbreviated as **UCAN**) and **CAN** have similar inhibition of PP2A [2e]. 5,6-dehydronorcantharidin (the unsaturated analogue of **DMC**, abbreviated as **UDMC**) and **DMC** still have similar inhibition of PP1, PP2A and PP2B [1f]. This suggests that **UCAN** and **UDMC** show similar anti-cancer and protein phosphatase activity as that of **CAN** and **DMC** (others think that the saturation of C5-C6 bond appears to affect the inhibitory activity, but not so crucial [5d]). More importantly, **UCAN** and **UDMC** are so easily synthesizable that they can often be used as

* Corresponding author. Tel.: +86 531 89631208; fax: +86 531 89631207; E-mail addresses: tanxuejie@163.com.

the starting material in the synthesis of **CAN** and **DMC** [10]. Then, what's the difference between 5,6-dehydronorcantharimide (the unsaturated analogue of **NCI**, abbreviated as **UNCI**) and **NCI**? Surprisingly, the derivatives based on **UNCI** have hardly been explored in the literature, much less than that of **UCAN** and **UDMC** analogues. Wang et al. found that the arylantimony derivatives based on **NCI** and **UNCI** have similar in vitro antitumor activities [11]. For example, the complexes $\mathbf{I_6}$, $\mathbf{I_7}$, and $\mathbf{II_7}$, $\mathbf{II_8}$ in their paper have very high and similar antitumor activities against some cancer cells (**Scheme 2**). Li et al. [12] have investigated the antiproliferative activities of ten **UNCI** and **NCI** derivatives (**Scheme 2**, **5a-5f**, **7a-7d**), which displayed moderate and similar inhibitory activities against A549 and PC-3 cell lines with the IC50 values >250.0 μmol/l (the IC50 of **DMC** were 44.8 and 201.0 μmol/l in their experiments). In one word, since **UNCI** and its analogues not only have simple chemical structures and less toxicity, but also retain the antitumor activities, is it possible for them to provide enormous possibilities for the science and industry of antitumor medicine? These uncertainties encourage us for further investigations related to these issues. We hope that these chemical modifications in the structure of **UNCI** could be a real and rapid way in developing new drug candidates.

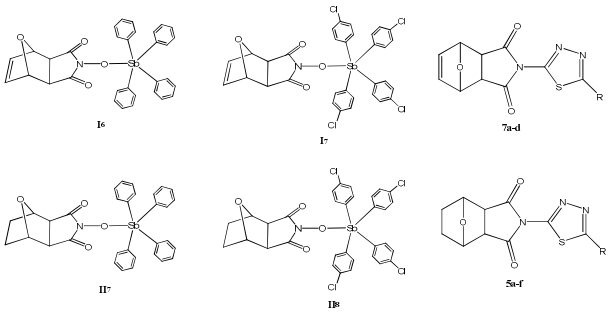

Scheme 2 Two sets of similar compounds with similar antitumor activities reported in reference [11] and [12]. Their name abbreviations are maintained as in the original report.

On the other hand, the dimer structure is ubiquitous in natural products and dimeric molecules would be expected to show enhanced receptor affinity relative to their corresponding monomeric counterparts [13]. Dimeric compounds have been synthesized and studied for the treatment of cancer, HIV, Alzheimer, malaria and various parasitic diseases [14]. McCluskey et al. [15] reported the synthesis and anticancer activities of two **NCI** dimers (**Scheme 3**, compounds **1** and **2**), which displayed the highest levels of cytotoxicity against a series of cell lines among 35 **NCI** derivatives that they synthesized. In addition, Noda et al [16] isolated three **CAI** dimers (**Scheme 3**, compounds **3** to **5**) from the Chinese blister beetle, *Mylabris phalerate* PALLAS (Meloidae). Their structures were determined based on spectroscopic and chemical evidence. But their cytotoxic activities were not demonstrated and have not been reported up to the present. The fourth example of **CAI** dimer is (3aR,3'aR,4S,4'S,7R,7'R,7aS,7'aS)-rel- 2,2'-[dithiobis(1,3,4-thiadiazole-5,2-diyl)]bis[hexahydro-3a,7a-dimethyl- 4,7-epoxy-1H-isoindole-1,3(2H)-dione (**Scheme 3**, compound **6**) reported by Kok et al [17]. The compound showed cytotoxic potential on the entire four cancer cell lines examined. The cytotoxic pattern of the dimer on carcinoma cell lines was similar to that of similar single state. The major difference between them was observed in KG1a, where the dimer was still effective at 12.5 μg/ml but a higher concentration was required for that of similar single state. Compared with these **NCI** and **CAI** dimers, we are unaware, however, of any studies about the detailed structure and potential biological activities based on **UNCI** dimmers.

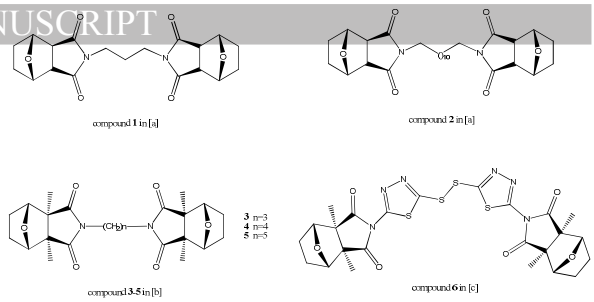

Scheme 3. The structures of some (nor)cantharimide (**NCI**/**CAI**) dimers reported in literature [15, 16, 17].

Another blank area is the crystal structure of the dimers. There have been no reports about the crystal structure of any **NCI**/**CAI** dimers. It is known that most small molecule drugs (>90%) are delivered in crystalline form [18] and at least half of marketed solid chemical drug substances exhibit polymorphism [19]. Meanwhile, medicinal chemistry requires robust reliable structures to accurately position key pharmacophoric units in the correct chemical space. It is this positioning that gives rise ultimately to the desired biological activity. To obtain a better understanding of the solid-state properties of these substances, it is necessary to identify and characterize crystal structures, and even to perform a polymorphic screening and physiochemical properties characterization, on potential drug candidates. This will help in eventually selecting a suitable form for further development and manufacturing. As part of our ongoing project studying novel unsaturated analogues of **DMC**/**NCI**, we have recently obtained systematical studies on a novel silver and singly protonated **UDMC** complex [20]. We now present our studies on the synthesis and thorough spectral and X-ray crystallographic characterization of four **UNCI** dimers (shown in **Scheme 4**). **UDMC-DETA** and **UDMC-TETA** are new; the rest two dimers have appeared before [21], but neither detailed structure information nor any properties have been reported. It is a substantial challenge to identify all these dimers' single-crystal structures because they are usually isolated as thin powders, which showed no tendency to crystallize. At last, all dimers are evaluated for their in vitro cytotoxic activity against two cancer cell lines, A549 (human lung cancer) and $4T_1$ (mouse breast cancer). Some interesting structure-activity relationships were observed.

The abbreviations and corresponding systematic names for four **UNCI** dimers formed between **UDMC** and butanediamine (**BDA**), 1.6-hexamethylendiamine (**HDA**), diethylenetriamine (**DETA**), triethylenetetramine (**TETA**) are as follows: **UDMC-BDA**, 2,2'-(1,4-butanediyl)bis(3a,4,7,7a-tetrahydro-4,7-epoxy-1,3-bishydroisoindole-1,3-dione); **UDMC-HDA**, 2,2'-(1,6-hexanediyl)bis(3a,4,7,7a-hexahydro-4,7-epoxy-1,3-bishydroisoindole-1,3-dione); **UDMC-DETA**, 2,2'-(3-aza-1,5-pentanediyl)bis(3a,4,7,7a-te-trahydro-4,7-epoxy-1,3-bishydroisoindole-1,3-dione); **UDMC-TETA**, 2,2'-(3,6-diaza-1,4-butanediyl)bis(3a,4,7,7a-te-trahydro-4,7-epoxy-1,3-bishydroisoindole-1,3-dione).

2 Experimental Section

2.1 Materials, synthesis and measurements

Chemicals, cell culture reagents and media were purchased from Aladdin-reagent Chemicals and were used without further purification.

Synthesis of **UDMC** follows methods in the literature [22]. Condensation of diamines with **UDMC** in anhydrous toluene or acetone gave the crude product **UNCI** dimers in around 20%

yield (**Scheme 4**). Though the dehydrative condensation of **DMC** with primary amines is the main methodology for the synthesis of **NCI** derivatives, no reports were found to synthesize **NCI**/**UNCI** dimers with this method. It should be noted that the temperature is a key factor in determining the end product. The yield will drastically decrease with increasing temperature and the major products will be various decomposition products and monomeric derivatives. The kinetic features associated with various products depend on the specific structure of the diamines, the reactant concentration, the medium and the temperature. These researches are ongoing and will be reported elsewhere.

The crude product was filtered, washed and then recrystallized with various solvents (see **Table S1** in the Supporting Information). All crystals are colorless with approximately long and thin bar shapes as shown in **Fig. S1** (in Supporting Information. All "**S**" numbered tables and figures are in Supporting Information). They are soluble in organic solvents such as methanol, ethanol, chloroform, acetonitrile, dimethyl formamide and dimethyl sulfoxide, but not soluble in toluene, acetone, ether, hexane and petroleum ether. The general reactions are shown as follows:

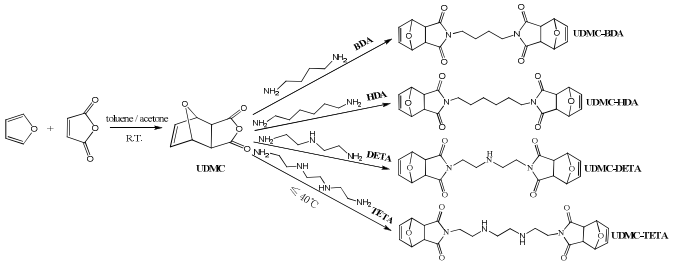

Scheme 4 The reaction sequence of four **UNCI** dimmers.

Elemental (C, H, N) analyses were carried out with a Perkin–Elmer 2400 microanalyzer. Accurate-mass measurements were acquired on an Agilent-6520 quadrupole-time of flight tandem mass spectrometer. ^{1}H and ^{13}C NMR spectra were run on a Bruker Avance 400 MHz instruments. The chemical shifts are reported in parts per million (ppm) relative to tetramethylsilane, $SiMe_4$ (δ = 0 ppm), referenced to the chemical shifts of residual solvent peak [deuterated dimethyl sulfoxide (DMSO-d6)]. UV–Vis absorption spectra were recorded using a UV-1700 spectrophotometer (Shimadzu, Japan), in 1×10^{-5}mol.L^{-1} acetonitrile or methanol solution. Infrared (IR) spectra were obtained as KBr pellets with a Bruker tensor 27 FT–IR spectrometer (Bruker, Germany). Melting points were determined on a WRS-2A electrothermal digital melting point apparatus (Shanghai precision & scientific instrument Co., Ltd, China).

The physico-chemical characterization results are listed below:

UDMC-BDA Elemental analysis: found (calc. for $C_{20}H_{20}N_2O_6$): C, 62.57 (62.49%); H, 5.31 (5.24%); N, 7.33 (7.29%); HRMS (ESI): *m*/*z* calcd for $C_{20}H_{20}N_2O_6$+H^+: 385.1400 [*M*+H^+]; found: 385.1404; M.p.165.0-166.0℃. ^{1}H NMR ($CDCl_3$): δ (ppm) 6.505(s, 4H, olefinic protons), 5.259(s, 4H, methine protons linked to bridge O, O-CH-), 3.484(s,4H, methylene protons linked to imide N, N-CH_2-), 2.834(s,4H, methine protons, -CH-), 1.549(s, 4H, methylene protons, -CH_2-). ^{13}C NMR ($CDCl_3$): δ (ppm) 175.687(carbonyl carbons), 136.020(olefinic carbons), 80.385(methine carbons linked to bridge O, O-CH-), 46.898(methine carbons, -CH-), 37.665(methylene carbons linked to imide N, N-CH_2-), 24.078(methylene carbons, -CH_2-). FT-TR(cm^{-1},KBr): 3076(m, ν C=C-H), 3011(m, ν C=C-H), 2963(m, ν C-H), 2930(m, ν C-H), 1769(s, ν C=O), 1705(vs, ν C=O), 1406(s, ν C-N), 1169(s, ν C-O-C); UV/Vis (CH_3CN) λmax/nm (ε/L·mol^{-1}·cm^{-1}): 214.0(3.5×10^5).

UDMC-HDA Elemental analysis: found (calc. for $C_{22}H_{24}N_2O_6$): C, 64.15 (64.07%); H, 5.91 (5.87%); N, 6.83 (6.79%); HRMS (ESI): *m*/*z* calcd for $C_{22}H_{24}N_2O_6$+H^+: 413.1713 [*M*+H^+]; found: 413.1711; M.p.158.8-159.4℃,.^{1}H NMR (DMSO):δ (ppm) 6.533(s, 4H, olefinic protons), 5.106(s, 4H, methine protons linked to bridge O, O-CH-), 3.297(s,4H, methylene protons linked to imide N, N-CH_2-), 2.894(s,4H, methine protons, -CH-), 1.384(t, J=6.4Hz,4H, methylene protons, -CH_2-), 1.225(s,4H, methylene protons, -CH_2-). ^{13}C NMR (DMSO): δ (ppm) 176.413(carbonyl carbons), 136.397(olefinic carbons), 80.283(methine carbons linked to bridge O, O-CH-), 47.034(methine carbons, -CH-), 37.700(methylene carbons linked to imide N, N-CH_2-), 26.798(methylene carbons, -CH_2-), 25.368(methylene carbons, -CH_2-). FT-TR(cm^{-1},KBr): 3069(w, ν C=C-H), 2995(m, ν C-H), 2930(m, ν C-H), 2859(w, ν C-H), 1771(s, ν C=O), 1697(vs, ν C=O), 1412(s, ν C-N), 1167(s, ν C-O-C); UV/Vis (CH_3CN) λmax/nm (ε/L·mol^{-1}·cm^{-1}): 207.0(2.2×10^5).

UDMC-DETA Elemental analysis: found (calc. for $C_{20}H_{21}N_3O_6$): C, 60.22 (60.14%); H, 5.41 (5.30%); N, 10.63 (10.52%); HRMS (ESI): *m*/*z* calcd for $C_{20}H_{21}N_3O_6$+H^+: 400.1509 [*M*+H^+]; found: 400.1513; M.p.126.0-127.2℃. ^{1}H NMR ($CDCl_3$): δ (ppm) 6.510(s, 4H, olefinic protons), 5.270(s, 4H, methine protons linked to bridge O, O-CH-), 3.556(t, J=6.0Hz, 4H, methylene protons linked to imide N, N-CH_2-), 2.859(s, 4H, methine protons, -CH-), 2.794(t, J=6.0Hz, 4H, methylene protons linked to secondary amino group, NH-CH_2), 2.097(s,1H, -NH-). ^{13}C NMR ($CDCl_3$): δ (ppm) 175.842(carbonyl carbons), 135.995(olefinic carbons), 80.323(methine carbons linked to bridge O, O-CH-), 46.943(methine carbons, -CH-), 45.673(methylene carbons linked to imide N, N-CH_2-), 38.175(methylene carbons linked to secondary amino group, NH-CH_2-). FT-TR(cm^{-1},KBr): 3333(s, ν N-H), 3084(w, ν C=C-H), 3014(w, ν C=C-H), 2953(m, ν C-H), 2812(m, ν C-H), 1767(s, ν C=O), 1711(vs, ν C=O), 1402(vs, ν C-N), 1204(s, ν C-O-C); UV/Vis (CH_3OH) λmax/nm (ε/L·mol^{-1}·cm^{-1}): 211.0(2.2×10^5).

UDMC-TETA Elemental analysis: found (calc. for $C_{22}H_{26}N_4O_6$): C, 59.84 (59.72%); H, 5.98 (5.92%); N, 12.73 (12.66%); HRMS (ESI): *m*/*z* calcd for $C_{22}H_{26}N_4O_6$+H^+: 443.1931 [*M*+H^+]; found: 443.1939; M.p.146.9-147.1℃. ^{1}H NMR (DMSO): δ (ppm) 6.535(s, 4H, olefinic protons), 5.107(s, 4H, methine protons linked to bridge O, O-CH-), 3.379(t, J=6.8Hz, 4H, methylene protons linked to imide N, N-CH_2-), 2.905(s, 4H, methine protons, -CH-), 2.559(t, J=6.8Hz,4H, methylene protons linked to secondary amino group, NH-CH_2), 2.480(s,4H, methylene protons linked to secondary amino group, NH-CH_2), 1.625(s, 2H, -NH-). ^{13}C NMR(DMSO): δ (ppm) 176.419(carbonyl carbons), 136.391(olefinic carbons), 80.291(methine carbons linked to bridge O, O-CH-), 48.282 (methylene carbons linked to imide N, N-CH_2-), 47.062(methine carbons, -CH-), 46.062(methylene carbons linked to secondary amino group, NH-CH_2-), 37.942(methylene carbons linked to secondary amino group, NH-CH_2-). FT-TR(cm^{-1},KBr): 3337(s, ν N-H), 3063(m, ν C=C-H), 3005(m, ν C=C-H), 2940(m, ν C-H), 2903(m, ν C-H), 2845(m, ν C-H), 1767(s, ν C=O), 1705(vs, ν C=O), 1404(s, ν C-N), 1177(s, ν C-O-C); UV/Vis (CH_3OH) λmax/nm (ε/L·mol^{-1}·cm^{-1}): 212.0(2.6×10^5).

2.2 X-Ray Crystallographic Analysis

The X-ray diffraction measurements were made on a Bruker APEX II CCD area detector diffractometer at 293K

for all **UNCI** dimers (Mo Ka radiation, graphite monochromator, λ = 0.71073 Å). The structures were solved by SHELXL-97. The absorption correction was done using the SADABS program [23]. Software packages APEX II (data collection), SAINT (cell refinement and data reduction), SHELXTL (data reduction, molecular graphics and publication material), DIAMOND (simplifying crystal packing diagram) were also used [24-26]. All non-hydrogen atoms were refined with anisotropic displacement parameters, and hydrogen atoms were placed in idealized positions and refined as rigid atoms with the relative isotropic displacement parameters.

2.3 Computational Study

In this work, theoretical calculations were mainly used to investigate spectral properties of all **UNCI** dimers.

In preliminary optimizations, the geometry of all dimers were first extracted from their single-crystal X-ray structures and then optimized by employing density functional theory (DFT) method with the B3LYP exchange correlation functional calculations [27, 28]. Frequency analyses have been made at the same level to ascertain the nature of the optimized structures to be the real minimum. Vertical electronic excitations based on B3LYP/6-31+G(d) optimized geometries were computed using the time-dependent density functional theory (TD-DFT) formalism [29] at the B3LYP/6-31+G(d) level. UV-Vis spectra as well as the assignment of vibrational modes (IR) were done on the basis of the GaussView 5.0 package [30]. The major contributions of the transitions were designated with the aid of SWizard program [31] using the Gaussian distribution model with the half-bandwidth of 500 cm^{-1} on the basis of TD-DFT results. DFT and TD-DFT calculations were carried out using the Gaussian03 program package [32] on a Sunway BlueLight MPP supercomputer housed at the National Supercomputer Center in Jinan, China.

2.4 Cytotoxicity Assays

Cell Culture. Human A549 (lung carcinoma) cells and mouse breast cancer 4T1 cells were purchased from Shanghai Cell Bank, Type Culture Collection Committee, Chinese Academy of Sciences. The cells were cultured in F12K medium supplemented with 10% heat inactivated fetal bovine serum (FBS), 2 mM glutamine, 100 U/mL penicillin, and 100 μg/mL streptomycin and maintained at 37 °C in humidified atmosphere of 5% CO_2.

MTT assay for cell proliferation. MTT assay was conducted and modified as described in the literature [33]. The cells (3000 cells) were seeded on 96-well microtitre plates in F12K medium with 10% FBS and incubated overnight. The cell culture medium was replaced by the different dose of compounds solution, and then the cells were cultured for another 72 h. The MTT [3-(4,5-dimethylthiazol-2-yl)-2,5-diphenyltetrazolium bromide] reagent was added to the cell supernatant for a final concentration of 0.5 mg/mL of MTT. After 3h the cell culture medium was removed. Formazan crystals in adherent cells were dissolved in 200 μL DMSO and the absorbance of the formazan solution was measured. Each compound was tested in triplicate and the experiments were repeated three times.

3 Results and Discussion

3.1 NMR characterization

In order to make the comparisons of NMR spectra between **UDMC** and **UNCI** dimers, the ^{1}H and ^{13}C NMR spectra of **UDMC** are listed in **Figs. S2** and **S3**. The ^{1}H and ^{13}C NMR spectra of four **UNCI** dimers are listed in **Figs. S4 - S11**.

In the ^{1}H NMR spectra of **UDMC**, the olefinic and methine protons all appear as singlet at δ = 6.567, 5.338 and 3.364 ppm, respectively (**Fig. S2**). When changing into **UNCI** dimers, they still appear as singlet, but all shift upfield (**Table S2**). For example, the olefinic protons of **UDMC-BDA** to **UDMC-TETA** are observed at 6.505, 6.533, 6.510 and 6.535 ppm, respectively. This can be attributed to the increasing shielding effect caused by the decreasing electronegativity from O to N, which makes electron density shift from imide N towards olefinic bond. In addition, protons that are nearer to the substituted N atom are shielded more. Similar shielding effect is observed in the ^{13}C NMR spectra, mainly supported by the significant shifts towards lower values of ppm (**Table S2**). For example, the two kinds of methine carbons are shielded by about 1.2 (the mean value of -1.304, -1.168, -1.259 and -1.14) and 1.4 (the mean value of -1.322, -1.424, -1.384 and -1.416) ppm respectively, relative to that in **UDMC**. The olefinic carbons are slightly shielded by only 0.3 ppm (the mean value of -0.455, -0.078, -0.48 and -0.084), because they are distant (at least 4.5 Å) from the N atom. As expected, the carbonyl carbon atoms should be greatly shielded due to their proximity to the N substitution (~ 1.38 Å). Surprisingly, relative to 169.3 ppm for **UDMC**, ^{13}C resonance frequencies shift towards higher values of 175.7, 176.4, 175.8 and 176.4 ppm in the dimer derivatives (from **UDMC-BDA** to **UDMC-TETA)** (**Table S2**). This 6.8 ppm (the mean value of 6.359, 7.085, 6.514 and 7.091) downfield shift reflects significant deshielding of the N substitution. Does N atom behave as shielding or deshielding towards the C atoms? This seems counterintuitive. It has been reported that intermolecular π-π interactions are responsible for this kind of deshielding as well as shielding of protons [34]. However, it seems that this supposition could not be used to explain the deshielding and shielding of carbon in **UNCI** dimeric (**Table S3**) and monomeric [22c, 35] derivatives. In addition, an attempt was made to check shielding/deshielding effect by calculating natural population analysis (NPA) and Mulliken [36] charges, which are shown in **Table S4**. However, calculated results show that N atom produces strong shielding instead of deshielding effect on carbonyl C. Of course, we are aware that atomic charges are not an observable quantum mechanical and these calculated values should be treated with a great deal of caution. After all, they are somewhat associated with the trend for electric field and electron population distributions. At last, we examined the crystal structure of **UDMC** and **UNCI** derivatives carefully and the coplanarity of O=C-N(O)-C=O group was analyzed systematically (**Table S5**). It can be seen that the two carbonyl groups are essentially coplanar with N/O atom and this coplanarity favors the existence of *p-π* conjugation. But the degree of coplanarity is decreased when O is changed into N. For example, the mean deviation is only 0.0034 Å for **UDMC**, but the values come to 0.0122-0.0387 Å after it is changed into **UNCI** derivatives. The deviation from coplanarity resulting from the N substitution means a reduction in the extent of *p-π* conjugation, which could be expected to level out the π-electron density, the signal for the carbonyl C atoms with π-electron-density deficit shifting downfield. This supposition was confirmed by similar reports in literatures [22c, 35], which are in line with their downfield shifting. In fact, many other instances of C=O group deshielding with breakdown of coplanarity and a reduction of conjugation effects are met in other compounds, such as the acyclic and alicyclic α, β-unsaturated ketones and aldehydes [37], unsaturated conjugated ω-amino-1,3-diketones and diesters [38]. Such an effect has never been explained before.

Briefly summarizing above, such a "remote-shielding *vis* near-deshielding" contradiction upon N substitution is believed to be the result of the decrease of coplanarity in the *p-π* electron conjugated system.

The secondary amino proton of **UDMC-DETA** resonated at 2.097 ppm and appeared as a broad singlet (**Fig. S6**). The integration of which indicates three protons instead of one, probably due to the water molecule in the crystal.

3.2 IR characterization

Based on the understanding of the relationship between experimentally observed frequencies and those DFT/B3LYP calculated results for the four strongest peaks (happen to be the most characteristic bands) in the IR spectrum of **UDMC**, we made assignments and analysis for the bands in the spectra of imide dimers.

Symmetric and antisymmetric stretches of C=O bond occur at 1859 and 1786 cm^{-1} in **UDMC** [39] (**Fig. S12**), but when **UDMC** is converted into imide dimers, no peak can be found in the region of 1860-1780 cm^{-1}, which are typical for saturated anhydrides in a 5-membered ring [40]. In their corresponding imide dimers, one band is located between 1771 and 1767 cm^{-1} (symmetric) and a more intense band occurs between 1721 and 1697 cm^{-1} (antisymmetric) (**Figs. S13 – S16**). The apparent shift of C=O vibration indicates the conversions of original anhydride into imide. Similar vibrational frequency ranges are reported in other references [41]. All the calculations for these imide dimers predict this shift (**Table S6**). For example, according to the values calculated with the DFT/B3LYP method, symmetric and antisymmetric stretches of C=O bond occur at 1918 and 1849 cm^{-1} in **UDMC**, but the corresponding frequencies in imide dimers are lowered to 1871 – 1831 cm^{-1} for symmetric vibrations and 1834 - 1767 cm^{-1} for antisymmetric vibrations. If proper value of the scale factor can be set (0.9631 in this work) [42], both the trend and the values of the shift are in good agreement with experimental results. The account of the shift reasonably lies in the 5-membered ring strain [39]. For a cyclic anhydride, the resonance within the -CO-O-CO- system causes it to be coplanar with the two carbonyls on the opposite side of the cyclic system. Similarly, the -CO-N-CO- system maintains the coplanar resonance in the cyclic imide. But the coplanarity is not as good as that in cyclic anhydride, which can be proved by their crystal structure (**Table S5**). Poor coplanarity and nitrogen substitution will decrease ring strain, thus shifting the two bands to lower frequencies. As for the intensity differences between the two bands (the symmetric stretching band is very weak relative to the antisymmetric stretching band), Yang and co-workers [39, 43] explained that the change in dipole moment of a 5-membered cyclic anhydride system for a symmetric stretching mode is small whereas that for an antisymmetric stretching mode is large. We think it can also be applied to the 5-membered cyclic imide system. Meanwhile, according to the DFT calculated results, the symmetric stretching band is indeed very weak relative to the antisymmetric stretching band, in line with the experimental results.

Again, the band shape of carbonyl antisymmetric vibration (1721 - 1697 cm^{-1}) is very diagnostic. The peak is broadened and asymmetric with implied or distinct shoulder at lower frequency side (**Figs. S12 – S16**), which arises from the overlap between C=C stretching mode and C=O antisymmetric vibration mode [44].

When C-O-C is converted into C-N-C in the formation of 5-membered cyclic imide, another two kinds of characteristic absorption bands undergo significant changes which can be a direct identification of this chemical reaction. The starting material (**UDMC**) shows two strong peaks at 1217 and 1088 cm^{-1} (**Fig. S12**), which arises from the C-O-C vibration in cyclic anhydride, the former is due to symmetric vibration and the latter is due to antisymmetric vibration [39]. But the corresponding frequencies in products (four **UNCI** dimers) shift to higher wavenumbers, *i.e.* 1412 - 1398 cm^{-1} for C-N-C symmetric vibrations and 1203 - 1165 cm^{-1} for C-N-C anti-symmetric vibrations. Both of them still have strong intensities. Krikorian *et al* and other groups [45 and the references therein] have found two similar spectral regions in simple cyclic imides, one at 1300-1400 cm^{-1} and another at 1030-1250 cm^{-1}. They believe that these two bands arise from mixed vibrationally coupled modes, *viz.* in-plane δ(N-H) and ν(C-N-C), with the symmetric C-N-C stretch contributing to the higher frequency and the antisymmetric C-N-C stretch to the lower. There are no N-H groups in the case of **UDMC-BDA** and **UDMC-HDA**, and the N-H bonds in **UDMC-DETA** and **UDMC-TETA** are far from the cyclic imide N atoms. So the two bands contain no contribution from the N-H vibrational component. Similarly, Grzetic and Oomens [46] have observed two strong bands at 1331 and 1235 cm^{-1} for glutarimide ring, which were assigned to the C-N-C symmetric and asymmetric stretching, excluding the N-H vibrational component. The computed spectra for the four imide dimers are in good accordance with the corresponding experimental spectra between 1000 and 1400 cm^{-1}. But the scale factor should be changed into 0.9946. In one word, the C-N-C stretching modes are essentially located in the range of 1412 - 1398 cm^{-1} for symmetric vibrations and 1203 - 1165 cm^{-1} for anti-symmetric vibrations. Both are very characteristic and most diagnostic for the assignment of N-substituted **UNCI** derivatives, since all four **UNCI** dimers present the same bands.

In the FTIR spectrum of **UDMC-TETA** (**Fig. S16**), an intense band of N-H stretching vibration at 3337 cm^{-1} is observed. The computed value is 3499.03 cm^{-1}, poorly reproduced by the calculations. The sharp, smooth shape of this band proves no interactions with any proton acceptors. But in the FTIR spectrum of **UDMC-DETA** (**Fig. S15**), the formation of an intramolecular hydrogen bond N3–H3B···O4 (**Table S11**, imine hydrogen bonded to the bended oxygen bridge) increase the distance between N and H, weakening the N-H bond and thus decreasing the vibrational frequency (red shift to 3333 cm^{-1}). Similarly, the computed value 3515.02 cm^{-1} does not agree with the experimental result. Despite the mismatch between experimental and DFT calculated spectra above 3000 cm^{-1}, the trend is accordant. Therefore, we can conclude that the hydrogen bond is the major contributor to the N-H band differences between **UDMC-TETA** and **UDMC-DETA**. Weak hydrogen bonding between the N3–H3B of the dimer bridge and the oxygen bridge redshifts the N−H stretch slightly and broadens it somewhat.

In summary, these **UNCI** dimers can be easily distinguished based on their IR spectra (*i.e.* the four strongest peaks plus N-H stretching modes in **UDMC-TETA** and **UDMC-DETA**).

3.3 Comparison of UV-Vis absorption spectra of UNCI dimers experimentally and theoretically

The observed electronic absorption spectra of four **UNCI** dimers (10^{-5} mol L^{-1} solution in CH_3CN or CH_3OH) are shown in **Fig. S17** with the maximum peak centered at 214, 207, 211 and 212 nm, respectively. The assignment of these electronic transitions can be performed with the help of theoretical calculations, which provide an in-depth understanding about their electronic structures and physical properties. This part presents

DFT/TD-DFT calculations of **UNCI** dimers' structure, electronic states and the main features for electronic absorption spectrum in gas phase as well as in proper solvents (the same solvents as those in experiments). Calculation results are in line with experimental data for all four dimmers (**Figs. S17 – S19**), but the degree of match-up is not very good in solvents with respect to those in gas phase. So the following analyses are mainly based on the gas phase, in which the lowest 30 singlet - singlet spin-allowed excitation states (all up to an energy of ~6.0 eV or ~190 nm) were taken into account for all calculations.

The geometry of four dimers used for calculations corresponds to their single-crystal X-ray structures. The optimized geometrical images and their single-crystal X-ray structures are compared and listed in **Fig. S20**. We notice that they have the same conformations and the same point groups.

To compare with experimental results, gas-phase UV-Vis absorption spectra are calculated. Excitation energies, oscillator strengths and corresponding electronic transition compositions for the simulated absorption bands are listed in **Table S7**. Within the near UV–Vis range, the strongest absorption oscillator strengths are found at 206.8, 205.8, 206.2 and 212.2 nm respectively, with small deviations between 0.2–7.2 nm. On the basis of these calculated match-up results, the transition mechanisms can be interpreted.

For **UDMC-BDA** (C_i point group), the main electron transitions of 214.0 nm (calculated result is 206.8 nm) come from transitions involving the HOMO/HOMO-1, and LUMO+3/LUMO+2, LUMO+1/LUMO orbitals (**Table S7**). HOMO and HOMO-1 are doubly degenerate with energy separated by only 0.0016 ev, both located in the C=O bonds (**Fig. S21**). LUMO+3 and LUMO+2, LUMO+1 and LUMO are another two sets of doubly degenerated orbitals with similar energies (separated by 0.0027 and 0.0079 ev, respectively), all localized over C=C bonds mixed with C=O bonds (**Fig. S21**). Therefore, this band can be assigned as the $\pi_{C=O} \rightarrow \pi^*_{C=C}$ mixed with $\pi_{C=O} \rightarrow \pi^*_{C=O}$ transitions.

Like **UDMC-BDA**, **UDMC-HDA** adopts C_i point group symmetry with the HUMO, HUMO-1 and HUMO-2 (the initial states of these transitions) being triply degenerate and localized over C=C and C=O bonds (**Fig. S22**). The LUMO follows a pair of degenerate LUMO+2 and LUMO+3 MOs, forming the final states of these transitions, which have a significant contribution from C=C and C=O bonds and negligible electron density on other atoms. Apparently, 207.0 nm (calculated 205.8 nm) is from $\pi \rightarrow \pi^*$ transitions.

Due to a lack of symmetry in **UDMC-DETA** (C_1 point group), the ground-state electronic structure contains little degeneracy and half parts of the molecule contain different MOs (**Figs. S23** and **S24**). According to the calculated results, there are two strong peaks above 200 nm, one at 206.2 nm and another at 238.1 nm. The intensity of the former is about three times stronger than the latter and they show different mechanisms. As the initial states of the transition at 206.2 nm, the high-lying occupied orbitals (HOMO-1 and HOMO-2) are quasi-degenerated orbitals with similar energy (-0.26865 and -0.26962 a.u. respectively), and mostly contributed by C=C and C=O bonds. LUMO+1, LUMO+2 and LUMO+3 orbitals (the final states of the transition at 206.2 nm) are still mainly composed of C=C and C=O bonds in antibonding arrangement. To some extent, this band represents $\pi \rightarrow \pi^*$ transitions. But the band around 238.1 nm is dominated by the single electron excitations from HOMO to LUMOs (LUMO+5, LUMO+4, LUMO+3). The distributions of the electronic states in these MOs can be seen in **Fig. S24**, where HOMO is localized over the bridging –NH– and $–CH_2–$ groups, away from the terminal bicyclo [2.2.1] skeletons. The largest orbital contributions of HOMO arise from the *2p* orbital of bridging N atom (around 69.78%) mixed with fewer characters of the *2p* orbital of four bridging C atoms (around 12.38%). The LUMOs are localized on the terminal bicyclo [2.2.1] skeletons and show a predominant character of $\pi^*_{C=O}$ and $\pi^*_{C=C}$ orbitals. So this band is largely originated from $n_N \rightarrow \pi^*$ transitions. In brief, the band observed at 211.0 nm, corresponding to the calculated band at 206.2 nm, can be assigned as the $\pi \rightarrow \pi^*$ transitions.

UDMC-TETA adopts approximate C_i symmetry. According to **Table S7** and **Fig. S18**, in the range of 240–200 nm, there are four strong excitation states (the *S*1 at 225.9 nm with $f = 0.1064$, the *S*2 at 215.5 nm with $f = 0.0451$, the *S*3 at 212.2 nm with $f = 0.0796$, and S4 at 205.1 nm with $f = 0.0698$). It can be seen from the plots (**Figs. S25-S28**) that the HOMO levels of S1, S2 and S3 are spread over the bridging $-(CH_2)_2$-NH-$(CH_2)_2$-NH-$(CH_2)_2$- group, mainly over the N atoms (are of *2p* orbital characterization), while the HOMO levels of S4 are localized over C=C bonds and bridging O atoms. The LUMOs (from LUMO+2 to LUMO+11) overall of these excited states are almost distributed over the whole molecule except some of the H atoms. It's worthy to be noted that the largest orbital contributions of two main LUMOs (LUMO+6 and LUMO+9) arise from NH (13.13% and 37.07%, respectively) and CH_2 (40.81% and 28.55%, respectively) fragments in the $-(CH_2)_2$-NH-$(CH_2)_2$-NH-$(CH_2)_2$- bridge, which can be regarded as $\sigma_{N\text{-}H}^*$ and $\sigma_{C\text{-}H}^*$ orbitals. So the observed band at 212 nm, corresponding to the calculated absorption band at 205-230 nm, which results from the superposition of four excitation states, can be assigned as many complicated transitions, mainly including $n_N \rightarrow \sigma_{N\text{-}H}^*$, $n_N \rightarrow \sigma_{C\text{-}H}^*$, $n_N \rightarrow \pi^*$ mixed with $\pi_{C=C} \rightarrow \pi^*$ transitions.

Thus far, only the calculated results in gas phase have been demonstrated and those in solvents have been omitted, because all match the experimental results well and the predicted transitions are similar. However, the spectral discrepancies between gas phase and solution are apparent for **UDMC-TETA**. In fact, the intrinsic transition mechanisms are different too. For example, there is only one strong peak above 200 nm. The calculated excitation energy, oscillator strength and the assignments of the transitions as well as the corresponding MO contour plots are shown in **Fig. S29**. Similar as that in gas phase, the initial states of the transition are spread over the bridging $-(CH_2)_2$-NH-$(CH_2)_2$-NH-$(CH_2)_2$- group, mainly over the N atoms (are of *2p* orbital characterization). But the final states are mainly localized on the cyclic imides, *i.e.* the π-*p*-π groups. So the excitation state at 217.8 nm with $f = 0.2237$, which mainly comes from the $n_N \rightarrow \pi^*$ transition, is responsible for the observed band centered at 212.0 nm.

In summary, both the dimer structures and the absorption spectra reproduced from theoretical calculations fit the experimental results well, so attempts to understand the nature of electronic transitions were carried out through comparison. Some important notes: 1) The transition mechanisms are different though showing some similarities; 2) The main bands in C_i symmetry compounds **UDMC-BDA** and **UDMC-HDA** are dominated by $\pi \rightarrow \pi^*$ transitions, where $\pi_{C=O} \rightarrow \pi^*$ plays the predominant role in **UDMC-BDA**; 3) **UDMC-DETA** has the lowest C_1 symmetry, and the main band can be assigned as the $\pi \rightarrow \pi^*$ transitions; 4) **UDMC-TETA** adopts approximate C_i symmetry and has the most complicated transition mechanism, which is most likely due to the introduction of another $-(CH_2)_2$-

NH- group, increasing the flexibility of the molecule and reducing the predictability of the resulting UV-Vis properties.

3.4 Crystal Structures of UNCI dimmers - Molecular Structure

The crystal structure of **UDMC** has been reported three times in 1972 [22a], 1998 [22b] and 2008 [22c]. Hundreds of its N-substituted derivatives (**UNCI**) have been synthesized but only about 22 of their structures (CCDC [47], Version 5.36, updated to May. 2015) have been confirmed through the X-ray diffraction analysis. No crystal structure of **NCI/UNCI** dimers can be found because they are not easy to form single crystals. Here, we report the single crystal data for four **UNCI** dimers.

A summary of the crystal data, experimental details and refinement results are given in **Table 1**. Molecular structures with atomic numbers of four **UNCI** dimers are depicted in **Fig. 1**. As can be seen from the figures, each polycyclic imide skeleton has the *exo*-conformation, which is more stable than the *endo*-structure and inevitably becomes the overwhelmingly major products under thermodynamic control [22c, 48].

Table 1 Crystallographic data and structure refinements summary for four **UNCI** dimers

Dimers	**UDMC-BDA**	**UDMC-HDA**	**UDMC-DETA**	**UDMC-TETA**
Chemical formula	$C_{20}H_{20}N_2O_6$	$C_{22}H_{24}N_2O_6$	$C_{20}H_{21}N_3O_6 \cdot H_2O$	$C_{22}H_{26}N_4O_6$
*M*r	384.38	412.43	417.41	442.47
Crystal habit	block/colorless	bar/colorless	bar/colorless	bar/colorless
Crystal system	monoclinic	monoclinic	triclinic	monoclinic
Space group	*P* $2_1/c$	*P* $2_1/n$	*P* -1	*P* 2_1
a /Å	11.362(3)	5.246(3)	8.765(3)	5.234(4)
b /Å	5.8986(17)	28.643(17)	9.709(3)	6.563(5)
c /Å	13.186(4)	6.546(4)	11.940(4)	30.52(2)
α /°	90.00	90.00	76.723(4)	90.00
β /°	98.318(4)	94.401(10)	78.423(4)	92.618(12)
γ /°	90.00	90.00	74.682(4)	90.00
V /Å^3	874.4(4)	980.8(10)	943.1(5)	1047.2(13)
Z	2	2	2	2
*D*calc. /g·cm^{-3}	1.460	1.397	1.470	1.403
μ /mm^{-1}	0.109	0.102	0.113	0.104
T /K	298	298	298	298
F(000)	404	436	440	468
*R*int	0.0405	0.0692	0.0615	0.0372
R_1 [$I>2\sigma(I)$]	0.0631	0.0545	0.0432	0.0758
wR_2/reflections	0.1335/1713	0.1057/1733	0.1118/3269	0.1878/3012
S	1.050	0.870	1.062	0.878

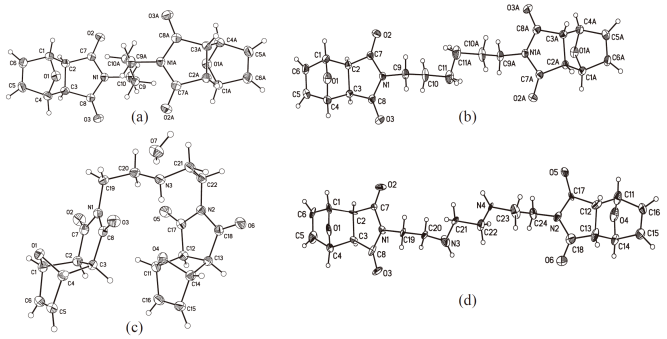

Figure 1. ORTEP view of four **UNCI** dimers with the atom numbering scheme. Displacement ellipsoids for non-H atoms are drawn at the 30% probability level. (a) **UDMC-BDA**, "A" represents the symmetry code of "−*x*, 1-*y*, 2−*z*" (For simplification, only one form of the disordered C10-C10A is shown); (b) **UDMC-HDA**, "A" represents the symmetry code of "3−*x*, -*y*, 1−*z*"; (c) **UDMC-DETA**; (d) **UDMC-TETA**.

Both **UDMC-BDA** and **UDMC-HDA** adopt C_i point group symmetry and both have an inversion center between the center two C atoms. Both contain one half-molecule in the asymmetric units and both have two formula units in the unit cell (Z=2). The former belongs to the space group *P21/c*, while the latter belongs to *P21/n*. Though the difference in the space group is due to the cell choice, the bridge -$(CH_2)_n$- (n=4 and 6) structure and the packing mode (will be discussed later) of the two **UNCI** dimers entirely differ. For **UDMC-BDA**, the propeller-like twisting between the **UNCI** units imparts chirality to the dimer, while **UDMC-HDA** exhibits an antigauche-gauche conformation without induction of any chirality (**Fig. 2**).

UDMC-DETA is a "weird" molecule in the following two parts. 1) The distance between two **UNCI** moieties is much shorter than that in other dimers (**Fig. 2**). It's only 5.3541(13) Å. We doubted the stability of this uncommon "U" type conformer and attributed its existence to the water molecule nearby. But when the experimental structure without H_2O was optimized using DFT/B3LYP method, the same kind of "U" type conformer was maintained in the final result. We began to realize that this conformer is stable with and without H_2O nearby. In fact, in order to confirm this supposition, we have checked many kinds of conformers. Conformation energy profiles for each single bond rotation are illustrated in **Fig. S30**, focusing on the energy variation of the gas phase **UDMC-DETA** as groups revolve around every single bond connection in the bridge chain. It was found that the energy barriers are very different for these single bond rotations (from 0.33 eV to 321.66 eV), which are not really "free", so the "U" type conformer is somewhat stable when it is established. On the other hand, most dihedral angles have wide adaptive range, which leads to a large number of relatively stable conformations. **Fig. S31** shows the comparison of two most stable conformers, along with the optimized "U" type conformer derived from the crystal structure, as well as the fourth

conformer with imposing C_2 point group symmetry. As can be seen, the "U" type conformer is one of the most stable conformers (the energy separation ≈ 0.00234 eV with the most stable one). 2) C_i point group symmetry constrains can't be placed on the dimer and only C_2 symmetry can be imposed to it, but the energy is about 0.125 eV higher than that of the most stable conformer (**Fig. S31**). Since chirality is the absence of inversion symmetry, it can be deduced that this mode of "twist disfavour" may impart chirality into the conformationally restricted dimer, which can be the origin of chirality in biarylamine units [49] and in some metal complexes [50].

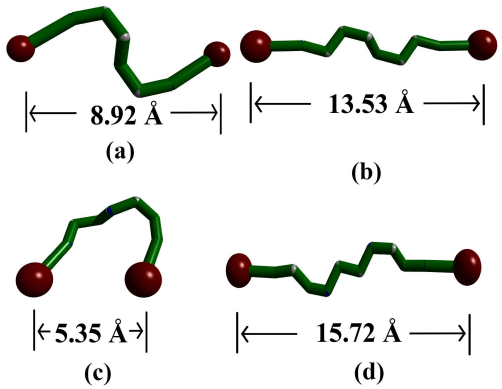

Figure 2. Simplified molecular structure of four **UNCI** dimers, illustrating different conformers of the bridge chains. Polycyclic imide skeleton except N is simplified by its center gravity (red balls at each end of the chains) and all H atoms have been omitted for clarity. (a) **UDMC-BDA**; (b) **UDMC-HDA**; (c) **UDMC-DETA** (water molecule has been omitted for clarity); (d) **UDMC-TETA**.

UDMC-TETA has the longest distance of 15.7178(67) Å between two **UNCI** moieties (**Fig. 2**), which is mainly because of the largest number of bridging atoms (8 atoms). As expected, the bridging chain has the maximum conformational flexibility, which can lead to subtle or dramatic changes in crystal structure, tending to reduce the predictability of the resulting assemblies. In the case of our studied crystal structure, the asymmetric unit contains one complete **UDMC-TETA** dimer and the dimer presents all antigauche conformation for three C-C single bonds. Moreover, the dimer has an inversion centre through the centre of the molecule. Surprisingly, such a centrosymmetric dimer crystallizes in the noncentrosymmetric polar, monoclinic space group *P2(1)* (No. 4), which is the only one of the four dimers crystallizing in a noncentrosymmetric space group. It is known that the presence of a centrosymmetric supramolecular synthon strongly tends toward centrosymmetric crystals [51]. However, a few examples [51, 52] indicate that the bulk crystal chirality can come from spatial disposition rather than the presence of chiral molecules themselves. In the case of **UDMC-TETA**, is the crystal chiral or achiral? This will be discussed in its packing structure.

In order to explore the skeleton changes when **UDMC** forms **UNCI** dimers, four dihedral angles (which can be regarded as one feature of similar skeletons) have been compared in **Table S8** on the basis of their crystal structures. It can be seen that the skeleton remains unchanged before and after the **UNCI** dimers' formation and the influence of environment (for example, hydrogen bonds) may cause a range-wide variation of some dihedral angles. For example, the angles between planes **C** and **D** can vary from 123.7° to 134.1° because of the presence or absence of hydrogen bonds. In most cases, plane **D** still does not bisect the angle between planes **B** and **C**. A tentative explanation for this might be the repulsive effect between the π-electrons of the C5-C6 double bond and non-bonding *p* electrons of the bridging oxygen atom [22a].

The last interesting thing to be noted is that, as highly twisted structures, **UDMC-BDA** and **UDMC-DETA** dimers are in fact helicate since they disfavor the twist [53]. As expected, **UDMC-HDA** and **UDMC-TETA** should have the same kinds of tendency in helicate formation with high induction of helicity. The thermodynamic conditions required for the formation of a single helicate remains elusive.

In brief summary, when the flexible single bond chains connect the rigid **UNCI** moieties into dimers, various conformers will be formed, including zigzag chains, "S" type and "U" type helicate chains, and often accompanied with the induction of helical chirality, which enable the possibilities of structure diversity and property multiplicity.

3.5 Crystal Structures of UNCI dimmers - Packing Structure

In the packing structure of the four dimers, no valuable π-π stacking interactions can be found and the dominant force is hydrogen bonding. The presence of various hydrogen bonding leads to quite interesting supramolecular architectures.

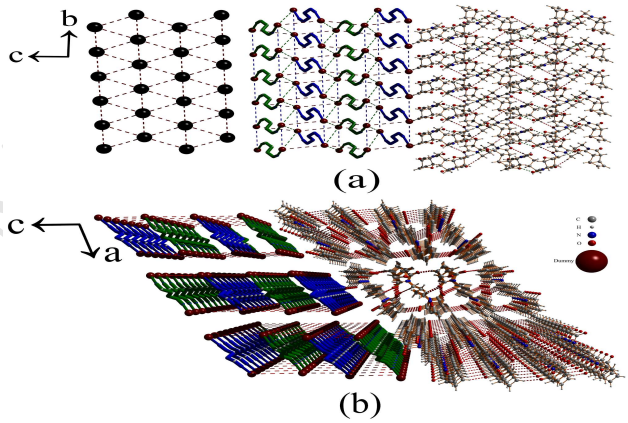

Figure 3. (a) 2D structure of **UDMC-BDA** formed by C-H…O interactions (shown red, green and blue dotted lines for three H-bonds respectively), view along the ***a*** axis. The middle one third is illustrated by the simplified dimers as used in **Fig. 2**, aiming to show different orientations (with blue and green colors, same in the blow). The left one third is further simplified by the center of gravity of all dimers, showing the two dimensional (3,6) topological diagram. **(b)** 3D structure formed by the packing of different 2D layers, view along the ***b*** axis.

UDMC-BDA is a 2D infinite layer framework formed by three kinds of C-H…O interactions (**Table S9**). Every hydrogen bond can link the dimer units into the same 2D layer structure, which extend parallel to the crystallographic ***bc*** plane. As can be seen in **Fig. 3a**, the repeated 2D rhomboid structures are composed of an interleaving arrangement of the M- and the P-forms of enantiomers. Although the dimer has a centrosymmetric space group (*P 21/c*) showing no chirality, the packing structure furnishes both the possible enantiomers, in which each dimer interacts with two adjacent dimers of opposite chirality by means of a moderate C-H…O hydrogen bonding interaction. If each **UDMC-BDA** dimer is simplified as a node, then their surrounding H-bonds can make them be simplified as a 6-connecting node, and the supramolecular layer has a two dimensional (3,6) net (**Fig. 3a**). But no hydrogen bond

interactions can be found between adjacent layers (**Fig. 3b**). So the layer structure is mainly maintained by van der Waals forces.

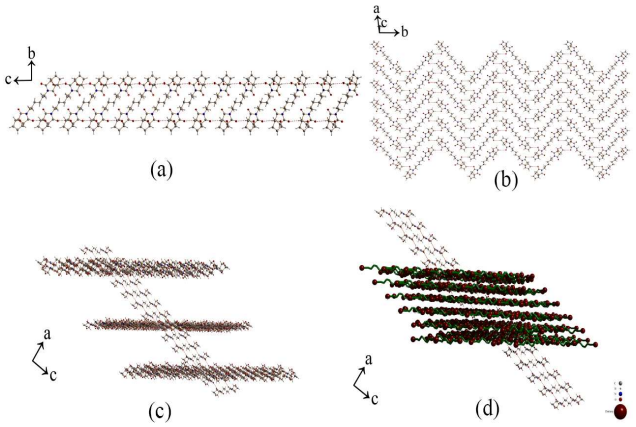

Figure 4. (a) Infinite 1D chain of **UDMC-HDA** formed through C–H…O H-bonds (shown red dotted lines), view perpendicular to the extending direction, *i.e.* ***c*** axis. **(b)** 2D structure formed by intermolecular C–H…O H-bonds, view perpendicular to the lying plane, *i.e.* **(1 0 -1)** crystal face. **(c)** 3D structure formed by the aforementioned (in **(a)** and **(b)**) two kinds of C–H…O H-bonds, view along the ***b*** axis. Only three discontinuous 2D layers (horizontal) and one chain (sloping) are shown for clarity. **(d)** Schematic illustration of the 3D structure view along the ***b*** axis.

There are two kinds of intermolecular C–H…O hydrogen bonds in **UDMC-HDA** (**Table S10**), both involves the same carbonyl O. But one H-bond (C3—H3···O2$^{(x,\ y,\ z-1)}$) link the dimers into 1D chains (**Fig. 4a**) and the other one (C6—H6···O2$^{(x-1/2,\ -y+1/2,\ z-1/2)}$) link the dimers into 2D layers (**Fig. 4b**). Then layers are further pillared by chains to generate 3D networks (**Figs. 4c** and **4d**). The dimers pack with a herringbone arrangement, so the layers show a zigzag alignment with each other parallel to **(1 0 -1)** crystal face. It seems that this packing is somewhat loose and contains large cavities, yielding the lowest crystal density of 1.397 g·cm^{-3} among the four **UNCI** dimers.

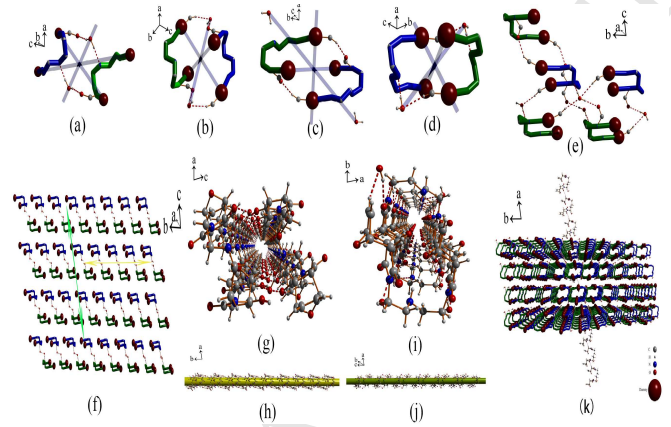

Figure 5. (a) Centrosymmetric supramolecular dimer containing two noncentrosymmetric **UDMC-DETA** dimers (a pair of enantiomers, shown in different colors) formed via H-bond O7—H7B···O6$^{(-x+1,\ -y,\ -z)}$. **(b)** Centrosymmetric supramolecular dimer formed via H-bond C5—H5···O7$^{(x,\ y+1,\ z)}$. **(c)** Centrosymmetric supramolecular dimer formed via H-bond C6—H6···O5$^{(-x+1,\ -y+1,\ -z+1)}$. **(d)** Centrosymmetric supramolecular dimer formed via H-bond C15—H15···O7$^{(-x+1,\ -y+1,\ -z)}$. **(e)** Four kinds of centrosymmetric supramolecular dimers present the basic supramolecular synthons, constituting the first step from molecules to crystals. **(f)** 2D structure formed by aforementioned supramolecular synthons, view perpendicular to the spreading plane, *i.e.* the crystallographic ***bc*** plane. Two arrows are used to show the formation of two kinds of channels. **(g)** End-on view of the crosssection of one channel inside the cage-like chain, view along the extending direction, *i.e.* ***b*** axis. **(h)** Packing diagram illustrating the aforementioned 1D cage-like chain, view perpendicular to the extending direction, *i.e.* ***b*** axis. **(i)** End-on view of the crosssection of another channel inside the cage-like chain, view along the extending direction, *i.e.* ***c*** axis. **(j)** Packing diagram illustrating the aforementioned 1D cage-like chain, view perpendicular to the extending direction, *i.e.* ***c*** axis. **(k)** Schematic illustration of the 3D structure view along the ***c*** axis.

As the least symmetric one among the four **UNCI** dimers, **UDMC-DETA** has the maximum probability to crystallize in a noncentrosymmetric lattice instead of its final space group *P-1*. So the current result may be contingent. But the packing structure analysis indicates that one water molecule makes centrosymmetric space group inevitable. **Table S11** shows that five kinds of intermolecular hydrogen bonds occur in the crystal structure (O7—H7A···N3 is also an intermolecular H-bond between water and **UDMC-DETA**, but it occurs in the same asymmetric unit. Though it is excluded from "five intermolecular H-bonds", this water-involved H-bond plays the most important role because the construction of most supramolecular dimers relys on it). Surprisingly, four kinds of them help to link noncentrosymmetric **UDMC-DETA** dimers into four kinds of centrosymmetric supramolecular dimers (**Figs. 5a-5e**), which in fact constitute the supramolecular synthons used to build up crystal architecture. This strongly indicates a loss of chirality during the presence of a centrosymmetric supramolecular synthon. These synthons are stacked together, first producing cage-like chains stretching along two directions (***b*** and ***c*** axis), and then leading to a 2D layer network lying the crystallographic ***bc*** plane (**Fig. 5f**). At last, the fifth kind of intermolecular hydrogen bonds (C12—H12···O3$^{(x+1,\ y,\ z)}$) bridge two adjacent layers to afford a 3D framework. Interestingly, two channels are formed within the 2D layer. One runs along the ***b*** axis and another along the ***c*** axis (**Figs. 5f -7j**), both inside the cage-like chains and running through the center of the assembly. The former is like an infinite rectangular tube with an effective crosssection 7.337×3.611 Å based on the shortest atom separation on opposite walls (**Figs. 5g, 5h**). The latter is also like an infinite rectangular tube but with two misaligned bridge O nearly separated it, in this end-on view the crosssection of the channel is approximately 7.795×3.723 Å with the narrowest neck about 1.912 Å (based on the shortest O…O separation) (**Figs. 5i, 5j**). Water molecules lie outside the channels and only be used to stabilize them through hydrogen bonds.

As is well known, the rational design and prediction of structures in solid state with the help of proper synthons formation are the main objectives of crystal engineering. In this sense, given that there is no water molecule in the crystal, **UDMC-DETA** could potentially result in structures with noncentrosymmetric lattice. But our attempts to prepare such crystal without water met with failure.

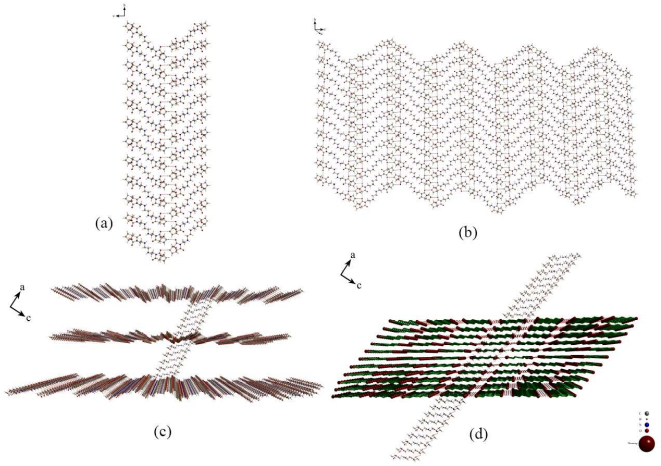

Figure 6. (a) Infinite 1D chain of **UDMC-TETA** formed through C6–H6…O2$^{(-x,\ y-1/2,\ -z)}$ H-bonds (shown red dotted lines), view perpendicular to the extending direction, *i.e.* ***b*** axis. **(b)** 2D structure formed by four kinds intermolecular C–H…O H-bonds, view perpendicular to the lying plane, *i.e.* **(1 0 -3)** crystal face. The four kinds of H-bonds are shown in different colors: blue C3—H3···O2$^{(x,\ y-1,\ z)}$; red C6—H6···O2$^{(-x,\ y-1/2,\ -z)}$; green C12—H12···O6$^{(x,\ y+1,\ z)}$; purple C15—H15···O6$^{(-x+3,\ y+1/2,\ -z+1)}$. **(c)** 3D structure formed by all five C–H…O H-bonds, view along the ***b*** axis. Only three discontinuous 2D layers (horizontal) and one chain (sloping) are shown for clarity. **(d)** Schematic illustration of the 3D structure view along the ***b*** axis.

There are five kinds of intermolecular hydrogen bonds in **UDMC-TETA** crystal (**Table S12**). Four involve carbonyl oxygens and they are approximately centrosymmetric, while the other one contains only one bridge oxygen (C13—H13···O4$^{(x-1,\ y,\ z)}$) in half part of the dimer. That's the reason why the dihedral angles of the skeleton are not symmetrically equal for **UDMC-TETA** (see "**3.4 Crystal Structures of UNCI dimmers - Molecular Structure**"). Each type of H-bonds results in the formation of 1D chains (**Fig. 6a**). The centrosymmetric four H-bonds work together to link **UDMC-TETA** dimers into 2D supramolecular layers (**Fig. 6b**). Within every layer, the dimers pack with a herringbone arrangement (similar as that in **UDMC-HDA**), so the layers show a zigzag alignment with each other parallel to **(1 0 -3)** crystal face (**Figs. 6b, 6c**). Subsequently, the H-bonds involving bridge oxygens further connect adjacent layers into 3D network (**Figs. 6c, 6d**). Still as that in **UDMC-HDA**, the crystal has the second lowest density (1.403 g·cm^{-3}), indicating this packing mode may be loose.

In the present structural analysis, another key feature is that such an approximately centrosymmetric dimer crystallize in a noncentrosymmetric polar space group ($P2_1$), which should be attributed to the "approximate" symmetry instead of "strict" one. But as we know, if the symmetry-related parts coexist in the asymmetric unit, they cannot be symmetrically identical. Then, does the slight asymmetry affect crystal structure? Or is the minor asymmetry influenced by crystal architecture? The question remains elusive for us now. Anyway, in the packing structure, we have not found chiral cavities, which can be formed through the packing of the molecules. And the detection of optical activity proves that **UDMC-TETA** is achiral. A few words about this topic: The space group $P2_1$ is often considered chiral space group (one of the 65 noncentrosymmetric Sohncke space group) [52h, 54], but the space group itself is achiral since it does not form one member of an enantiomorphous pair, even though a crystal structure in $P2_1$ can be chiral [52a].

Taken together, all four **UNCI** dimers pack as layers in the crystal, and the layers are connected only by van der Waals forces in **UDMC-BDA**, or by H-bonds as well (in **UDMC-HDA**, **UDMC-DETA** and **UDMC-TETA**). It appears that the interstitial space between the layers cannot be efficiently filled and the distances between adjacent layers are significantly different (**Fig. S32**). This leads to a very different crystal density (from 1.397 to 1.470 g·cm^{-3}) and all lower than that of **UDMC** (1.550 g·cm^{-3}). It's worthy to be noted that two **UNCI** dimers (**UDMC-BDA**, **UDMC-DETA**) have chirality but the presence of dimer units with opposite chirality makes the crystal achiral. Another interesting phenomenon is that approximately centrosymmetric **UDMC-TETA** crystallizes in a noncentrosymmetric space group $P2_1$. It can be deduced from our analysis that the molecular conformation and crystal structure have lots of possibilities, those reported here are just random ones.

3.6 Antitumor evaluation ─Inhibition of lung/breast cancer cell growth

To study the growth inhibitory effects of four **UNCI** dimers on lung cancer and breast cancer cells, we treated human A549 and mouse $4T_1$ cells with compounds and examined the growth of cells with MTT assay. To gain further evidence for their antitumor activities, the anti-proliferative activities of the saturated analogues **DMC-BDA** and **DMC-HDA**, which were prepared from **UDMC-BDA** and **UDMC-HDA** by catalytic hydrogenation, were also determined. Meanwhile, the experiments were carried out with **UDMC**, **DMC** and cisplatin for comparison.

Table 2. Inhibition of A549 and $4T_1$ cells growth by four **UNCI** dimers, compared with similar compounds.

compounds	A549 cells growth inhibition, IC_{50} (μM)	$4T_1$ cells growth inhibition, IC_{50} (μM)
UDMC-BDA	> 100	> 100
UDMC-HDA	> 100	> 100
UDMC-DETA	> 100	> 100
UDMC-TETA	> 100	> 100
DMC-BDA	> 100	> 100
DMC-HDA	94.0 ± 2.0	89.0 ± 1.0
UDMC	> 100	> 100
DMC	49.0 ± 0.9	46.0 ± 0.7
cisplatin	6.6 ± 0.6	0.5 ± 0.08

The cytotoxic activities as 50% inhibitory concentration (IC50) values are shown in **Table 2**. It can be seen that in A549 and 4T1 cells, all four **UNCI** dimers and one **NCI** dimers as well as **UDMC** are inactive (show no noteworthy cytotoxicity at 100 μM drug dose). Only **DMC-HDA** shows modest cytotoxicity. McCluskey et al. [15] have reported two **NCI** dimers, one is propyl-linked bisnorcantharimide, another is dodecyl-linked bisnorcantharimide (**Scheme 3**, compounds **1** and **2**), and their cytotoxic effects against a panel of nine human cancer cell lines were investigated by MTT assay. Even though the nine cancer cell lines are different from the two in our experiment, the results are somewhat similar. Propyl-linked **NCI** dimer shows very weak cytotoxicities (Inhibition ratio (%) at 100 μM drug concentration ranges from 10 ± 7 to 52 ± 41), much less potent than the dodecyl-linked analogue (GI50 ranges from 8.3 ± 0.7

μM to 60 ± 6 μM). Some interesting structure-activity relationships are disclosed: of all the dimers, twelve CH_2 groups linked dimer shows the best cytotoxic activity, six CH_2 groups linked dimer shows only moderate cytotoxicity, while three and four CH_2 groups linked dimers are likewise inactive. In this sense, we could observe that the longer chain, the higher therapeutic efficacy for **NCI** dimers. Long chain linked dimers appear to be endowed with cytotoxic activity, though the reason is still unclear.

S. H. Li et al. [12] have reported the antiproliferative activities of a series of ten **UNCI** and **NCI** derivatives (**Scheme 2**, compounds **5a-f**, **7a-d**), which displayed moderate and similar inhibitory activities against A549 and PC-3 cell lines. But the IC50 values of **UNCI** series are a little higher than that of their **NCI** analogues. Another important reference is J. S. Li' paper [11], in which they studied in vitro antitumor activities of fifteen arylantimony derivatives based on **UNCI/NCI**. The structures of four most cytotoxic derivatives (**I_6**, **I_7**, **II_7** and **II_8**) are listed in **Scheme 2**. The inhibition ratio against six cancer cell lines at 10 μg/ml drug concentration for **I_6** range from 6.9 to 74.5%, while from 38.6 to 87.6% for **II_7**, indicating **NCI** derivatives (**II_7**) have stronger inhibitory activity than **UNCI** analogues (**I_6**). At the same time, the inhibition ratio range from 84.8 to 97.3% for **I_7**, and from 33.6 to 92.2% for **II_8**, indicating **UNCI** derivatives (**I_7**) have higher inhibitory activity than **NCI** analogues (**II_8**). When considering the results of our present research, **DMC-HDA** shows modest cytotoxicity, while **UDMC-HDA** is inactive. It may be deduced that the double bond between C5, C6 positions may slightly inhibit cytotoxic activity in most cases.

Presumably in vitro antitumor properties of **UNCI/NCI** dimers depend mainly on the length of link chains and have something to do with the double bond (5,6-ene), but this hypothesis requires more **UNCI** and **NCI** dimer analogues with exact structure information as well as additional biologically evaluations. These works as well as detailed investigations focusing on cytotoxicity in several different types of cancer cells (some **CAN** analogues show more specific inhibitory and cytotoxic activities on both the Hep3B HCC and the KG1a AML cell lines, but their cytotoxic effects were weaker on both A549 lung cancer and MDA-MB231 breast cancer [17]) and the mechanisms of action are ongoing.

It is still earlier to summarize the situation in the context of **UDMC**/**DMC** dimers modification. Because, we still have only learned what not to do if one wishes to improve its anti-tumor activities (for example, one should avoid to change the bridging O atom) rather than what one must aim for in order to ensure improved bioactivities, for example, the bonding properties (saturated or unsaturated), the length of link chains, the solubility, charge, chirality, crystal structure, conformation (*exo*-, *endo*-, etc.) and the degree of polymerization (dimer or monomer). But our preliminary data provide entity to study these structural factors associated with biological activities.

4 Conclusions

In this paper we report the synthesis and characterization of four **UNCI** dimers, in which two **UNCI** units are linked with four and six CH_2 groups or -$(CH_2)_2$-NH-$(CH_2)_2$- and -$(CH_2)_2$-NH-$(CH_2)_2$-NH-$(CH_2)_2$- chains. To compare with the experimental results, UV-Vis, IR spectra and the relationships between conformation and energy were investigated by theoretical calculations.

The structural elucidation and the complete NMR assignment of the four dimers were performed. When **UDMC** is changed into **UNCI** dimers, the signals of olefinic and methine protons in ^{1}H NMR spectra all shift upfield, due to the shielding effect of substituted N atom. Similar shielding effect is observed in the ^{13}C NMR spectra for olefinic and methine carbons. But the carbonyl carbon is always deshielded with respect to their starting material **UDMC**, which does not agree with traditional theory and DFT calculated results. In this paper, we explained the shielding/deshielding contradiction, which is attributed to the decrease of coplanarity in the O=C-N(O)-C=O *p*-π conjugated system.

Inspection of the four experimental IR spectra and comparison with the starting material and with their corresponding theoretical spectra leads to the conclusion that the four most intense peaks are diagnostic and they can characterize the formation of the cyclic imide rings: 1771 - 1767 cm^{-1} (C=O of cyclic imide anti-symmetric stretching), 1721 - 1697 cm^{-1} (C=O of cyclic imide symmetric stretching), 1412 - 1398 cm^{-1} (C-N-C symmetric vibrations) and 1203 - 1165 cm^{-1} (C-N-C anti-symmetric vibrations).

UV-Vis absorption spectra of the four **UNCI** dimers were reproduced from TD-DFT calculations, which match the experimentally obtained spectra. Attempts to understand the nature of electronic transitions were carried out through comparison. All together our data, the main bands in the dimers are dominated by $\pi \rightarrow \pi^*$ mixed with $n \rightarrow \pi^*$ transitions and the detailed transition mechanisms are different.

The single crystals of a series of **UNCI** dimers enable us to compare their molecular and crystal structures systematically. Comparison of the molecular assemblies in the crystals clearly demonstrated that only small structural differences in a molecule, that is, the number of CH_2 or NH groups in link chains, cause a significant change in the assembly in the crystalline state. **UDMC-HDA** and **UDMC-TETA** exhibit common antigauche-gauche conformation without induction of any chirality, but **UDMC-BDA** and **UDMC-DETA** present "S" type or "U" type helicate configurations with chirality. When packing into crystals, both helicates crystallize into centrosymmetric lattice with the loss of chirality, but approximately centrosymmetric **UDMC-TETA** packs into noncentrosymmetric polar space group ($P2_1$) though still without chirality. In their crystal packing structures, supramolecular synthons *via* conventional hydrogen bonds have been analyzed and the common feature is that 2D layer structures are formed. There have been no reports in which such subtle link group effects in crystals of dimeric molecules were systematically analyzed and, therefore, the present system can contribute to the design of desired functional crystalline materials.

Cell viability assay demonstrated that these four **UNCI** dimers were ineffective death inducers in human A549 and mouse $4T_1$ cells and control experiments with their saturated analogues indicated that only **DMC-HDA** shows modest cytotoxicity. By comparing with the relevant results obtained from the literature, a preliminary conclusion suggests that the antitumor properties of **UNCI/NCI** dimers depend mainly on the length of link chains (the longer chain, the higher therapeutic efficacy) and have something to do with the double bond (in most cases, **NCI** derivatives suppress tumor growth more effectively than **UNCI** analogues). To clarify the biological role of link chains, we next plan to synthesize various and longer chains linked **UNCI/NCI** dimers based on this model. Meanwhile, a two-step assembly process is invoked as a way of rationalizing the observed structures and we will pursue the crystal structures of corresponding saturated dimers in order to shed more light on the precise similarities/differences in their

supramolecular structures. We expect that the unambiguous structure will help to illustrate the whole structure-activity relationship deeply.

Acknowledgments

The authors are thankful to the Science & Technology Development Projects of Shandong Province in China (No. 2011GGX10706 and 2012GGX10702) and the National Natural Science Foundation of PR China (NSFC, No. 21103100) for financial support. Generous support in computing resources from the National Supercomputer Center in Jinan, China, is greatly appreciated.

Supplementary Material

Supplementary Information available: **Tables S1** to **S12**, **Figures S1** to **S32** mentioned in the text. Crystallographic information files of four **UNCI** dimers. CCDC < 1446287, 1446288, 1446289 and 1446290> contains the supplementary crystallographic data for < **UDMC-BDA, UDMC-HDA, UDMC-DETA** and **UDMC-TETA** >. These data can be obtained free of charge from The Cambridge Crystallographic Data Centre via http://www.ccdc.cam.ac.uk/data_request/cif , or from the Cambridge Crystallographic Data Centre, 12 Union Road, Cambridge CB2 1EZ, UK; fax: (+44) 1223-336-033; or e-mail: deposit@ccdc.cam.ac.uk.

References and notes

[1] (a) I. Bertini, V. Calderone, M. Fragai, C. Luchinat, E. Talluri, *J. Med. Chem.* **2009**, *52*, 4838; (b) Y. M. Li, J. E. Casida, *Proc. Natl. Acad. Sci. U.S.A.* **1992**, *89*, 11867; (c) J. Knapp, P. Boknik, S. Huke, I. Gombosova, B. Linck, H. Luss, F. U. Muller, T. Muller, P. Nacke, W. Schmitz, U. Vahlensieck, J. Neumann, *Gen. Pharmacol*, **1998**, *31*, 729; (d) A. McCluskey, J.A. Sakoff, *Mini. Rev. Med. Chem*, **2001**, *1*, 43; (e) Y. Baba, N. Hirukawa, N. Tanohira, M. Sodeoka, *J. Am. Chem. Soc*, **2003**, *125*, 9740; (f) M. Sodeoka,Y. Baba,S. Kobayashi, N. Hirukawa, *Bioorg. Med. Chem. Lett*, **1997**, *7*, 1833; (g) S. G. Stewart, T. A. Hill, J. Gilbert, S. P. Ackland, J. A. Sakoff, A. McCluskey, *Bioorganic & Medicinal Chemistry*, **2007**,*15*, 7301.

[2] (a) T. Efferth, R. Rauh, S. Kahl, M. Tomicic, H. Bo¨chzelt, M. E. Tome, M. M. Briehl, R. Bauer, B. Kaina, *Biochemical Pharmacology*, **2006**,*69* ,811; (b) X. Wang, S. C.F. Au-Yeung, Y.P. Ho, *Journal of Inorganic Biochemistry*, **2007**,*101*,909; (c) Y.P. Ho, K.K.W. To, S.C.F. Au-Yeung, X. Wang, G. Lin, X. Han, *J. Med. Chem.*, **2001**, *44*, 2065; (d) G. S. Wang, J Ethnopharmacol, **1989**, *26*, 147; (e) L.P. Deng, J. Dong, H. Cai, W. Wang, *Current Medicinal Chemistry*,**2013**, *20*, 159; (f) F. Peng, Y. Q. Wei, L. Tian, L. Yang, X. Zhao, Y. Lu, Y. Q. Mao, B. Kan, S. Lei, G. S. Wang, Y. Jiang, Q. R. Wang, F. Luo, L. Q. Zou, J. Y. Liu, *Cancer Res. Clin. Oncol.*, **2002**, *128*, 223; (g) Y.J. Chen, C.D. Kuo,Y.M. Tsai, C.C. Yu, G.S. Wang, H.F. Liao, *Anti-Cancer. Drugs*, **2008**, *19*, 55; (h) Y. N. Chen, J. C. Chen, S. C. Yin, G. S. Wang, W. Tsauer, S. F. Hsu, S. L. Hsu, *Int. J. Cancer*, **2002**, *100*, 158; (i) L. A.Williams, W. Moller, E. Merisor, W. Kraus, H. Rosner, *West. Ind. Med.J*., **2003**, *52*, 10; (j) J. E. Huh, K. S. Kang, C. Chae, H. M. Kim, K. S. Ahn, S. H. Kim, *Biochem Pharmacol*., **2004**, *67*, 1811; (k) J. Z. Wu, Z. Q. Situ, J. Y. Chen, B. Liu, W. Wang, *Chin. Med. J*., **1992**, *105*, 1026; (l) S. H. Kok, C. H. Chui, W. S. Lam, J. Chen, J. C. Tang, F. Y. Lau, G. Y. Cheng, R. S. Wong, A. S. Chan, *Int. J. Mol. Med.*, **2006**, *17*, 945; (m) S. H. Kok, C. H. Chui, W. S. Lam, J. Chen, J. C. Tang, F. Y. Lau, G. Y. Cheng, R. S. Wong, A. S. Chan,*Int. J. Mol. Med*., **2006**, *18*, 1217; (n) W. Li, L. Xie, Z. Chen, Y. Zhu, Y. Sun, Y. Miao, Z. Xu, X. Han, *Cancer Sci*., **2010**, *101*, 1226; (o) L. C. Nicholls, D. Teare, *Br. Med. J.* **1954**, *2*, 1384; (p) P. Y. Lin, S. J. Shi, F. L. Hsu, C. F. Chen, *J. Chin. Chem. Soc. (Taipei, Taiwan)* **1998**, *45*, 323.

[3] R. Rauh,S. Kahl,H. Boechzelt, R. Bauer,B. Kaina, T. Efferth, *Chinese Medicine*, **2007**, *2*, 1.

[4] (a) K. K. W. To, Y. P. Ho, S. C. F. Au-Yeung, *J. Chromatogr. A.* **2002**, *947*, 319; (b) Y. P. Ho, S. C. F. Au-Yeung, K. K. W. To, *Med. Res. Rev*., **2003**, *23 (5)*, 633; (c) K. K. W. To, X. Wang, C. W. Yu, Y. P. Ho, S. C. F. Au-Yeung, *Bioorg. Med. Chem.* **2004**, *12*, 4565; (d) K. K. W. To, Y. P. Ho, S. C. F. Au-Yeung, *Cancer Lett*, **2005**, *223*, 227; (e) C. W. Yu, K. K. W. Li, S. K. Pang, S. C. F. Au-Yeung, Y. P. Ho, *Bioorg. Med. Chem. Lett.* **2006**, *16*, 1686; (f) S. C. F. Au-Yeung, P. S. K. Pang, Y. P. Ho, *Nat. Rev. Drug Discov*., **2006**, *5*, 5; (g) S. K. Pang, C. W. Yu, S. C. F. Au-Yeung, Y. P. Ho, *Biochem. Biophys. Res. Commun*, **2007**, *363*, 235; (h) S. K. Pang, C. W. Yu, S. C. F. Au-Yeung, Y. P. Ho, *Oncol. Reports*, **2008**, *20*, 1269.

[5] (a) A. Tan, B. Koc, E. Sahin, N. H. Kishali, Y. Kara, *SYNTHESIS*, **2011**, 7, 1079; (b) P. Y. Lin, S. J. Shi, H. L. Shu, H. F. Chen, C. C. Lin, P. C. Liu, L. F. Wang, *Bioorganic Chem*, **2000**, *28*, 266; (c) I. J. Tseng, S. Y. Sheu, P. Y. Li, J. A. Lee, K. L. Ou, L. W. Lee, *J Exp Clin Med*, **2012**, *4*, 280; (d) C. E. P. Galvis, L. Y. V. Méndez, V. V. Kouznetsov, *Chem. Biol. Drug. Des*, **2013**, *82*, 477; (e) B. Sauer, J. Gilbert, J. A. Sakoff, A. McCluskey, *Lett. Drug Des. Discov*. **2009**, *6*, 1; (f) M. J. Robertson, C. P. Gordon, J. Gilbert, A. McCluskey, A. Jennette, J. A. Sakoff, *Bioorg Med Chem*, **2011**, *19*, 5734.

[6] A. McCluskey, M. C. Bowyer, E. Collins, A. T. R. Sim, J. A. Sakoff, M. L. Baldwin, *Bioorg. Med. Chem. Lett*, **2000**, *10*, 1687.

[7] A. McCluskey, C. Walkom, M. C. Bowyer, S. P. Ackland, E. Gardiner, J. A. Sak.

[8] W. Tsauer, J. G. Lin, P. Y. Lin, F. L. Hsu, H. C. Chiang, *Anticancer Res*,**1997**, *17*, 2095.

[9] (a) A. McCluskey, S. P. Ackland, M. C. Bowyer, M. L. Baldwin, J. Garner, C. C. Walkom, J. A. Sakoff, *Bioorg Chem*, **2003**, *31*, 68; (b) A. McCluskey, A. T. Sim, J. A. Sakoff, *J Med Chem*, **2002**, *45*, 1151; (c) M. E. Hart, A. R. Chamberlin, C. Walkom, J. A. Sakoff, A. McCluskey, *Bioorg. Med. Chem. Lett*, **2004**, *14*, 1969; (d) A. McCluskey, M. A. Keane, L. M. Mudgee, A. T. Sim, J. Sakoff, R. J. Quinn, *Eur J Med Chem* **2000**, *35*, 957.

[10] M. C. Chang, E. T. Tsai, J. Y. Wu, H. F. Liao, Y. J. Chen, C. D. Kuo, *Anti-Cancer Drugs*, **2015**, *26*, 5, 508.

[11] G. C. Wang, J. Xiao, L. Yu, J. S. Li, J. R. Cui, R. Q. Wang, F. X. Ran, *J Organomet Chem*, **2004**, *689*, 1631.

[12] G. G. Tu, J. F. Zhan, Q. L. Lv, J. Q. Wang, B. H. Kuang, S. H. Li, *Med. Chem.* **2014**, *10*, 376.

[13] P. S. Portoghese, *J. Med. Chem.* **1992**, *35*, 1927.

[14] B. Gervais, Current Medicinal Chemistry, **2006**, 13, 131.

[15] T. A. Hill, S. G. Stewart, S. P. Ackland, J. Gilbert, B. Sauer, J. A. Sakoff, A. McCluskey, *Bioorg Med Chem*, **2007**,*15*, 6126.

[16] T. Nakatani, K. Jinpo, N. Noda, *Chem. Pharm. Bull*, **2007**, *55* (1), 92.

[17] S. H. L. Kok, C. H. Chui, W. S. Lam, J. Chen, J. C. O. Tang, F. Y. Lau, G. Y. M. Cheng, R. S. M. Wong, A. S. C. Chan, *Int J Mol Med*, **2006**, *17*, 151.

[18] N. Variankaval, A. S. Cote, M. F. Doherty, *American Institute Of Chemical Engineers*, **2008**, *54*, 1682.

[19] G. P. Stahly, *Cryst. Growth. Des*. **2007**, *7*, 1007.

[20] (a) F. Y. Wang, X. B. Jiang, X. J. Tan, D. X. Xing, *Acta Crystallogr.* C67, **2011**, m218; (b) S. P. Li, S. Zhang, X. Jin, X. J. Tan, J. F. Lou, X. M. Zhang, Y. X. Zhao, *Eur. J. Med. Chem*, **2014**, 86, 1; (c) X. Jin, X. J. Tan, X. M. Zhang, M. Y. Han, Y. X. Zhao, *Bioorg. Med. Chem. Lett*, **2015**, *25*, 4477.

[21] V. Rao, S. Navath, M. Kottur, J. R. McElhanon, D. V. McGrath, *Tetrahedron Lett*, **2013**, *54*, 5011.

[22] (a) S. Baggio, A. Barriola, P. K. de Perazzo, *J.Chem.Soc.*,*Perkin Trans*, **1972**, *2*, 934; (b) B. M. Ramirez, G. D. de Delgado, W. O. Velasquez, G. M. Perdomo, *Z. Kristallogr.- New Crystal Structures*,**1998**, *213*, 197; (c) Y. W. Goh, B. R. Pool, J. M. White, *J.Org.Chem.*,**2008**, *73*, 151.

[23] G. M. Sheldrick, SADABS, Bruker AXS Inc., Madison, Wisconsin, USA, **2004.**

[24] G. M. Sheldrick, *Acta Crystallogr, Sect. A*, **2008**, 64 112.

[25] Bruker APEX II (version 2.0-1), SAINT (version 7.23A), XPREP (version 2005/2), SHELXTL (version 6.1). Bruker AXS Inc., Madison, Wisconsin, USA, **2005**.

[26] K. Brandenburg, H. Putz, DIAMOND. Crystal Impact GbR, Bonn, Germany, **2005**.

[27] A. D. Becke, *J. Chem. Phys.* **1993**, *98*, 5648.

[28] C. Lee, W. Yang, R. G. Parr, *Phys. Rev. B: Condens. Matter Mater. Phys.* **1988**, *37* ,785.

[29] (a) R. Bauernschmitt, R. Ahlrichs, *Chem. Phys. Lett.* **1996**,*256*, 454; (b) R. E. Stratmann, G. E. Scuseria, M. J. Frisch, *J. Chem. Phys*., **1998**, *109*, 8218; (c) M. E. Casida, C. Jamorski, K. C. Casida, D. R. Salahub, *J. Chem. Phys*, **1998**, *108* , 4439.

[30] A. B. Nielsen, A. J. Holder, *GaussView, User´s Reference*, GAUSSIAN, Inc.: Pittsburgh, PA, USA **1997-1998**.

[31] (a) S. I. Gorelsky, *SWizard Program* Revision 4.6; University of Ottawa: Ottawa, Canada, **2010**; http://www.sg-chem.net/. (b) S. I. Gorelsky, A. B. P. Lever, *J. Organomet. Chem.* **2001**, *635*, 187.

[32] M. J. Frisch, G. W. Trucks, H. B. Schlegel, G. E. Scuseria, M. A. Robb, J. R. Cheeseman, J. A. Jr. Montgomery, T. Vreven, K. N. Kudin, J. C. Burant, J. M. Millam, S. S. Iyengar, J. Tomasi, V. Barone, B. Mennucci, M. Cossi, G. Scalmani, N. Rega, G. A. Petersson, H. Nakatsuji, M. Hada, M. Ehara, K. Toyota, R. Fukuda, J. Hasegawa, M. Ishida, T. Nakajima, Y. Honda, O. Kitao, H. Nakai, M. Klene, X. Li, J. E. Knox, H. P. Hratchian, J. B. Cross, V. Bakken, C. Adamo, J. Jaramillo, R. Gomperts, R. E. Stratmann, O. Yazyev, A. J.Austin, R. Cammi, C. Pomelli, J. W. Ochterski, P. Y. Ayala, K. Morokuma, G. A. Voth, P. Salvador, J. J. Dannenberg, V. G. Zakrzewski, S. Dapprich, A. D. Daniels, M. C. Strain, O. Farkas, D. K. Malick, A. D. Rabuck, K. Raghavachari, J. B. Foresman, J. V. Ortiz, Q. Cui, A. G. Baboul, S. Clifford, J. Cioslowski, B. B. Stefanov, G. Liu, A. Liashenko, P. Piskorz, I. Komaromi, R. L. Martin, D. J. Fox, T. Keith, M. A. Al-Laham, C. Y. Peng, A. Nanayakkara, M. Challacombe, P. M. W. Gill, B. Johnson, W. Chen, M. W. Wong, C. Gonzalez, J. A. Pople, *Gaussian 03*, revision C.02; Gaussian, Inc.: Wallingford, CT, **2004**.

[33] Y. Zhao, W. Liu, Y. Zhou, X. Zhang, P. V. Murphy, *Bioorg. Med. Chem. Lett*. **2010**, 20, 7540.

[34] M. Majumder, N. Sathyamurthy, *Theor Chem Acc*, **2012**, *131*, 1092.

[35] (a) L. A. Mitchell, J. M. Stanley, L. E. De Hoyos, B. J. Holliday, *Acta Crystallogr.,Sect.C (Cr.Str.Comm.)*, **2013**, *69***,** 638; (b) T. Fallon, A. C. Willis, M. N. Paddon-Row, M. S. Sherburn, *J.Org.Chem.*, **2014**, *79***,** 3185.

[36] A. E. Reed, F. J. Weinstock, *Chem. Phy*, **1985**, *83*, 735.

[37] D. H. Marr, J. B. Stothers, *Can. J. Chem.*,**1965**, *43*, 596.

[38] E. P. Prokof'ev, Zh. A. Krasnaya, *Russian Chemical Bulletin*, **1978**, *27***,** 10**,** 2037.

[39] X. Gu, C. Q. Yang, *Res. Chem. Intermed.*, **1998**, *24*, 979.

[40] N. B. Colthup, L. H. Daly, S. E. Wiberley, *Introduction to Infrared and Ramon Spectroscopy*, Academic Press, New York. **1975**, pp 297, 308.

[41] (a) P. T. McKitfrick, J. E. Katon, *Appl. Spectrosc.* **1990**, *44*，812; (b) H. Niu, M. Huang, S. Qi, E. Han, G. Tian, X. Wang, D. Wu, *Polymer*, **2013**, *54*, 1700; (c) M. Zhang, H. Niu, J. Chang, Q. Ge, L. Cao, D. Wu, *Polym. Eng. Sci.* **2015**, 2615-2625; (d) I. N. Tarabara, A. O. Kas'yan, M. Yu. Yarovoi, S. V. Shishkina, O. V. Shishkin, L. I. Kas'yan, *Russ. J. Org. Chem.* **2004**, *40*, 992. In (b), (c) and (d), the authors believe asymmetic stretching lies in higher wavenumbers, which maybe wrong according to our calculated results and other relevant references.

[42] X. J. Tan, H. Z. Liu, C. Z. Ye, J. F. Lou, Y. Liu, D. X. Xing, S. P. Li, S. L. Liu, L. Z. Song , *Polyhedron*，**2014**, *71*, 119.

[43] C. Q. Yang, G. Zhang, *Res. Chem. Intermed.*, **2000**, *26*, 515.

[44] P. A. Okafor, B. Huxel, J. O. Iroh, *J. Appl. Polym. Sci*. **2015,** DOI: 10.1002/APP.42673.

[45] P. J. Mcneilly, T. A. Andrea, S. E. Krikorian, *Spectrochim. Acta* A, **1992**, *48*, 1437.

[46] J. Grzetic, J. Oomens, *J. Am. Soc. Mass Spectrom*, **2013**, *24*, 1228.

[47] F. H. Allen, *Acta Crystallogr. B*, **2002**, *58*, 380.

[48] (a) M. W. Lee, W. C. Herndon, *J. Org. Chem.* **1978**, *43*, 518; (b) P. X. Iten, A**.** A. Hofmann, C. H. Eugster, *Helv. Chim. Acta*, **1979**, *62*, 2202.

[49] C. J. Sanders, K. M. Gillespie, D. Bell, P. Scott, *J. Am. Chem.Soc.*, **2000**, *122*, 7132.

[50] (a) X. Sun, D. W. Johnson, D. L. Caulder, K. N. Raymond, E. H. Wong, *J. Am. Chem. Soc*., **2001**, *123*, 2752; (b) A. M. Garcia-Deibe, J. S. Metalobos, M. Fondo, M. Vazquez, M. R. Bermejo, *Inorg. Chim. Acta*, **2004**, *357*, 2561; (c) X. Sun, D. W. Johnson, K. N. Raymond, E. H. Wong, *Inorg. Chem.*, **2001**, *40*, 4504; (d) Y. P. Cai, C. Y. Su, C. L. Chen, Y. M. Li, B. S. Kang, A. S. C. Chan, W. Kaim, *Inorg. Chem*., **2003**, *42*, 163; (e) W. Schuh, H. Kopacka, K. Wurst, P. Peringer, *Eur. J. Inorg. Chem*., **2002**, 2202; (*f*) M. Albrecht, I. Janser, H. Houjou, R. Frohlich, *Chem.-Eur. J*., **2004**, *10*, 2839; *(g*) M. Albrecht, *Chem.-Eur. J*., **1997**, *3*, 1466; (h) S. P. Argent, H. Adams, T. Riis-Johannessen, J. C. Jeffery, L. P. Harding, W. Clegg, R. W. Harrington, M. D. Ward, *Dalton Trans*., **2006**, 4996.

[51] B. Moulton, M. J. Zaworotko, *Chem. Rev*. **2001,** *101*, 1629.

[52] (a) C. Janiak, A. Chamayou, A. K. M. R. Uddin, M. Uddin, K. S. Hagen, M. Enamullah, *Dalton Trans.*, **2009**, 3698; (b) T. Hang, D. W. Fu, Q. Ye, R. G. Xiong, *Cryst. Growth Des*. **2009**, *9*, 2026; (c) Q. Ye, T. Hang, D. W. Fu, G. H. Xu, R. G. Xiong , *Cryst. Growth Des.* **2008**, *8*, 3501; (d) C. J. Sumby, J. Fisher, T. J. Prior, M. J. Hardie, *Chem. Eur. J*. **2006**, *12*, 2945; (e) Q. Sun, Y. Bai, G. He, C. Duan, Z. Lin, Q. Meng**,** *Chem. Commun*., **2006**, 2777; (f) R. W. Saalfrank, H. Maid, F. Hampel, K. Peters, *Eur. J. Inorg. Chem.* **1999**, 1859; (g) O. Mamula, A. Von Zelewsky, T. Bark, G. Bernardinelli, *Angew. Chem., Int. Ed. Engl.* **1999**, *38*, 2945; (h) T. Ezuhara, K. Endo, Y. Aoyama, *J. Am. Chem. Soc.* **1999**, *121*, 3279; (i) K. Biradha, C. Seward, M. Zaworotko, J. *Angew. Chem., Int. Ed. Engl.* **1999**, *38*, 492; (j) C. Kaes, M. W. Hosseini, C. E. F. Rickard, B. W. Skelton, A. H. White, *Angew. Chem., Int. Ed. Engl*, **1998**, *37*, 920; (k) D. Whang, J. Heo, C. A. Kim, K. Kim, *Chem. Commun.* **1997**, 2361; (l) E. Psillakis, J. C. Jeffery, J. A. McCleverty, M. D. Ward, *Dalton Trans.* **1997**, 1645; (m) M. A. Withersby, A. J. Blake, N. R. Champness, P. Hubberstey, W. S. Li, M. Schroder, *Angew. Chem., Int. Ed. Engl.* **1997**, *36*, 2327; (n) M. C. Hong, W. P. Su, R. Cao, M. Fujita, J. X. Lu, *Chem. Eur. J*. **2000**, *6*, 427; (o) W. W. Ellis, M. Schmitz, A. A. Arif, P. Stang, J. *Inorg. Chem.* **2000**, *39*, 2547; (p) J. D. Ranford, J. J. Vittal, D. Q. Wu, X. D. Yang, *Angew. Chem., Int. Ed. Engl.* **1999**, *38*, 3498; (q) W. Jaunky, M. W. Hosseini, J. M. Planeix, A. De Cian, N. Kyritsakas, Fischer, J. *Chem. Commun.* **1999**, 2313.

[53] J. M. Lehn, A. Rigault, J. Siegel, J. Harrowfield, B. Chevrier, D. Moras, *Proc. Natl. Acad. Sci. U. S. A.* **1987,** *84*, 2565.

[54] (a) K. Matsuda, S. Yamamoto, M. Irie, *Tetrahedron Lett.*, **2001**, *42(41)*, 7291-7293; (b) W. G. Lu，J. Z. Gu，L. Jiang，M. Y. Tan，T. B. Lu, *Cryst. Growth & Des.*, **2007**, *8*, 192; (c) Z. Chen, Y. Su, W. Xiong, L. Wang, F. Liang, M. Shao, *CrystEngComm*, **2009**, *11*, 318; (d) P. M. Selvakumar, E. Suresh, P.S. Subramanian**,** *Polyhedron*, **2009,** *28*, 245; (e) H. Wu, X. Dong, H. Liu, J. Ma, Y. Liu, Y. Liu, J. Yang**,** *Inorg. Chim. Acta*, **2011**, *373*, 19.

.

Highlights

1) Four unsaturated norcantharimide dimers were synthesized and well characterized.

2) Single crystal structure studies have been carried out, which is the first report about the crystal structures of cantharidin derivative dimers.

3) Introduction of various lengths of single bond chains provides high conformational flexibility, which can afford unusual structures and interesting biological activities.

4) In vitro antitumor evaluations indicate that the antitumor properties of dimers depend on the length of link chains.